SONOLUMINESCENCE AND ACOUSTICALLY DRIVEN OPTICAL PHENOMENA IN SOLIDS AND SOLID–GAS INTERFACES

I.V. OSTROVSKII[a], O.A. KOROTCHENKOV[a,b], T. GOTO[b], H.G. GRIMMEISS[c]

[a]*Faculty of Physics, Taras Shevchenko Kiev University, Kiev 252022, Ukraine*
[b]*Department of Physics, Graduate School of Science, Tohoku University, Sendai 980, Japan*
[c]*Solid State Physics, University of Lund, Box 118, S-221 00 Lund, Sweden*

ELSEVIER

AMSTERDAM – LAUSANNE – NEW YORK – OXFORD – SHANNON – TOKYO

ELSEVIER

Physics Reports 311 (1999) 1–46

PHYSICS REPORTS

Sonoluminescence and acoustically driven optical phenomena in solids and solid–gas interfaces

I.V. Ostrovskii[a], O.A. Korotchenkov[a,b,*], T. Goto[b], H.G. Grimmeiss[c]

[a] *Faculty of Physics, Taras Shevchenko Kiev University, Kiev 252022, Ukraine*
[b] *Department of Physics, Graduate School of Science, Tohoku University, Sendai 980, Japan*
[c] *Solid State Physics, University of Lund, Box 118, S-221 00 Lund, Sweden*

Received July 1998; editor: D.D. Awschalom

Contents

Abstract

During the last decade, significant progress has been achieved in our understanding of the generation of light in acoustic fields, a research area which is known as sonoluminescence (SL). Some of the data obtained, including SL effects in water, have previously been reviewed in the literature. This article takes a broader view and reports on experimental evidence of SL phenomena in solids and solid–gas interfaces as well as on interpretations and potential applications. It is shown that the understanding of SL is facilitated when couched in the language of moving dislocations which produce vacancy–interstitial pairs of host atoms. Radiative transitions in defect pairs would then constitute the SL effect in solids. It is further shown that the occurrence of electric fields due to the generated point defects and charged dislocations produces a number of interesting phenomena. These fields are particularly important for the occurrence of SL at

* Corresponding author. Faculty of Physics, Taras Shevchenko Kiev University, Kiev 252022, Ukraine. E-mail: olegk@tower.ups.kiev.ua.

PII: S0370-1573(98)00079-9

solid–gas interfaces which has been suggested to be initiated by gas discharges due to strong electric fields of charged dislocations. The appearance of acoustically driven internal electric fields is shown to lead to remarkable effects with regard to exciton lifetimes. The storage of photogenerated electron–hole pairs in the moving piezoelectric potential of acoustic waves allows prolonged exciton recombination times of μs in InGaAs/GaAs quantum well structures. The intertwining of acoustically driven long-range electric fields and microfields occurring at the exciton sites turns out to be a prerequisite for attaining the lifetime tuning of the bound excitons in CdS crystals. The review is concluded by discussing sonoluminescence effects in granular systems. Implications for the relevance of this effect to the dynamical behavior of granular media are outlined.

PACS: 78.60.Mq; 71.55. − i; 52.80. − s; 83.70.Fn; 71.35. − y

Keywords: Sonoluminescence; Acoustic driving; Defect charge; Gas discharge; Granular dynamics; Exciton lifetime

1. Introduction

Sonoluminescence (SL), the conversion of acoustic energy into light, satisfies the criteria for fundamentality and interdisciplinarity, thus proving the present interest in this research area which is sustained both in condensed matter physics and technology applications. However, almost half a century after its discovery in water (Marinesco and Trillat, 1933; Frenzel and Schultes, 1934), there was little activity in this field. Most experiments suffered from emission instabilities and the lack of proper measurement techniques.

In recent years, the SL phenomenon emerged as a subject of remarkably increased interest to physicists. Substantial progress has been made due to the observation of SL in solids (Ostrovskii et al., 1979; Miyake and Futama, 1982). Very recently, further progress has been achieved owing to the discovery of a single bubble SL in water (Gaitan et al., 1992). A single gas bubble trapped in a resonant sound field has been shown to produce synchronized pulses of light with a clocklike regularity. Though essential differences in the appearance of SL have been observed in liquids and solids, the light production is generated in both cases by similar complex effects which are governed either by bubble or dislocation dynamics.

Although our insight into SL has been improved considerably, new discoveries generate still further mysteries. An example of this is the open question, why acoustic waves with a quantum energy less than 10^{-9} eV can cause the emission of light with typical energies of more than 1 eV. Despite uncertainties regarding the fundamental physical mechanism, there is no doubt that SL requires a concentration of acoustic energy in small volumes of a medium. This explains the resulting high local temperatures and pressures which are of great interest for future applications. It has, for example, been suggested to use these properties for fusion (Barber et al., 1994; Moss et al., 1996) although its realization yet remains a challenging task. On the other hand, the impact of acoustic energy concentration on chemical reactions has gradually been recognized and is widely employed in sonochemistry technologies which actually represent a unique interaction of energy and matter.

The increasing interest in sonoluminescence research yielded recently a series of interesting reviews (e.g. Walton and Reynolds, 1984; Crum, 1994; Barber et al., 1997) which, however, were mostly focused on sonoluminescence phenomena in water. In this article, we shall examine sonoluminescence effects in solids and granular mixtures as well as at solid–gas interfaces. Hence, one objective of this review is to discuss sonoluminescence studies in a broader perspective than previous reviews by treating this phenomenon in various kinds of matter: solids, liquids, gases and granular materials. Granular materials have frequently been considered as an additional state of matter.

We shall also point out new areas of acoustically affected optical phenomena by showing that the concept of acoustic driving has recently resulted in important payoff effects. Some examples in this context are (1) the acoustically driven storage of light in InGaAs/GaAs quantum well structures which opened a wide field for novel acoustooptic devices (Rocke et al., 1997); (2) acoustically driven net charges at crystal defects which lead to enhanced long-range electric fields governing optical phenomena (Ostrovskii and Rozhko, 1984; Ostrovskii and Das, 1997); (3) the variation of the local crystal environment of defect sites (Korotchenkov and Grimmeiss, 1995) which is capable of tuning the lifetime of photogenerated carriers captured at defect centers (Korotchenkov and Goto, 1998a).

Our presentation is organized as follows. After a brief overview of sonoluminescence of cavitation bubbles in water in Section 2, sonoluminescence and acoustically driven photoconductivity as well as optical absorption in solids are discussed in Section 3. Though a large number of studies

have been performed in a large variety of materials, the discussion in Section 3 is restricted to materials such as CdS and ZnS semiconductors. A running idea through this presentation is the remarkable change of defect concentrations as well as net charges of point defects and dislocations at sufficiently high driving amplitudes. It will be illustrated how these changes influence optical processes which in turn are indicative of material properties imposed by external parameters. In Section 4, we introduce the sonoluminescence of gases adjacent to the surface of crystals which drive acoustic waves. The data obtained with $LiNbO_3$/air and CdS/He interfaces provide evidence for irradiation effects of atoms and molecules adsorbed at the crystal surface. It is shown that simple models of gas discharges in the piezoelectric field of acoustic waves cannot be applied and that certain implications have to be considered within the framework of acoustically driven net charges at crystal defects. The sonoluminescence in granular materials of ZnS and ZnS : Mn particles is discussed in Section 5. A key issue of this discussion is the interplay of the observed sonoluminescence and granular dynamics. We illustrate this within the approach of granular "fluid" which is shown to give an accurate account of the observations. In Section 6, a discussion of acoustically driven excitonic effects is performed. Our considerations are centered around the acoustically affected radiative lifetime in InGaAs/GaAs quantum wells and bound excitons in CdS crystals. The physics behind these effects is based on electric fields accompanying acoustic driving. It will be shown how the radiative lifetime of excitons is increased by orders of magnitude in quantum wells. It is further demonstrated that the intertwining of the acoustically driven long-range electric fields and short-range interatomic forces can provide both increased and decreased lifetimes of bound excitons. A brief summary given in Section 7 concludes our presentation.

2. Overview of sonoluminescence in liquids

Sonoluminescence in liquids is generated due to the growth and collapse of gas-filled bubbles induced by sound fields. A typical experimental arrangement for the observation of SL consists of a water-filled round bottom flask driven at its fundamental resonant frequency with piezoelectric transducers that are mounted at opposite poles of the flask. If the acoustic pressure in the water is high enough, multibubble sonoluminescence (Marinesco and Trillat, 1933; Frenzel and Schultes, 1934) can arise from bubbles of various sizes. To obtain single bubble SL (Gaitan et al., 1992), a single bubble of gas is placed into the water and kept in place by trapping the bubble in a resonant sound field. Such SL has been found to be highly reproducible and to exhibit very enhanced brightness when compared to that of multibubble SL. As the acoustic-pressure amplitude is varied, the gas bubble goes through a number of states that eventually lead to SL (Wu and Roberts, 1993; Putterman, 1995). The bubble starts to expand from a radius of several μm due to a drop in acoustic pressure and increases to a maximum radius of about 50 μm. When the acoustic cycle becomes compressive, the bubble collapses violently to about 0.5 μm.

SL is generally believed to be caused by rapid compression of gas inside collapsing cavitation bubbles but the details of this mechanism are still not understood. One example of these uncertainties is the surprisingly short duration of SL flashes of the order of picosecond (Barber et al., 1994; Gompf et al., 1997). These timescales are difficult to explain by conventional theories of cavitation bubble collapse with predicted timescales a thousand times higher (Crum and Roy, 1994) than those detected. This difficulty has led to the development of the classical theory of shock waves

(Wu and Roberts, 1993) which are observed when the collapsing bubble well attains supersonic velocities. These microshocks converge at the core of the gas bubble to create a very short-duration compression. The gas inside the bubble is heated by the shock waves and achieves such high temperatures that it becomes ionized and leads to SL from the plasma. Temperatures as high as 10^6 K and even higher are often assumed in the framework of the microshock model.

Spectroscopic measurements have granted useful insights into the nature of SL. Typical SL spectra exhibit broadbands with the highest intensity in the ultraviolet region (Frommhold and Atchley, 1994; Matula et al., 1995; Hiller and Putterman, 1995; Barber et al., 1997). The broadband nature of the spectra and the observation of an emission peak in the ultraviolet suggest that the SL bubble indeed is very hot. However, the featureless spectra of SL can in many cases be explained by various processes such as blackbody radiation, bremsstrahlung from accelerating free electrons, chemiluminescence due to molecular dissociation or even more exotic processes. Examples of these are cracking of the ice shell that forms on the bubble wall due to the solidification at very high pressures (Hickling, 1994) and fracturing of the water that cannot flow when stressed with sufficient intensity and rapidity (Prosperetti, 1997). Physicists are still searching for the fundamental mechanism responsible for SL in liquids since existing theories in most cases fail to predict hitherto unknown properties implying serious limitations of our present understanding of SL. Although a great deal of controversy exists about the question whether or not SL effects in liquids and solids can be explained from a universal point of view, we nevertheless believe that the existing theories of SL in water may provide a good starting point for a better understanding of this phenomenon since the microfracturing of a crystal lattice is an essential feature of the SL in solid matter, as will be demonstrated in the next section.

3. Sonoluminescence and acoustically driven optical effects in solids

3.1. Observing sonoluminescence

Increasing the acoustic energy flux above a certain threshold value results in some crystals SL effects. By far the largest number of such studies have employed II–VI semiconducting compounds and alkali halide crystals (see e.g. Ostrovskii et al., 1979, 1983; Miyake and Futama, 1982; Zhmurko et al., 1983; Korotchenkov and Goto, 1997). In a few cases, however, other solid materials such as $LiNbO_3$ and $Bi_{12}GeO_{20}$ have also been used (Lysenko and Ostrovskii, 1981b; Ostrovskii and Lysykh, 1985).

Several techniques are currently available that can provide high enough acoustic fields in solids for observing SL. A simplified setup of the experimental configuration used to observe SL in piezoelectric crystals is illustrated in Fig. 1. Two pairs of metal electrodes are deposited on both sides of the plate-shaped sample. Vibrations inside the piezoelectric sample are excited by applying an rf electric voltage U to one pair of the electrodes, whereas the other pair serves as a detector of transmitting vibrational responses. Both the cw and toneburst drivings have been found to be capable to produce the SL effect in a certain driving voltage – frequency range. As a practical consequence, the frequency of the driving voltage is swept through a range of a large number of plate modes corresponding to Lamb and shear horizontal waves. These waves propagate parallel to the surface of the plate (Viktorov, 1967; Solie and Auld, 1973) which eventually leads to the appearance of SL in narrow regions of sufficiently intense acoustic fields.

In some experiments, a pair of piezoelectric transducers has been attached to opposite faces of nonpiezoelectric samples, usually parallelepipeds, to generate ultrasonic vibrations which travel back and forth across the sample. An example of such a sample–transducer arrangement is shown in Fig. 2. The externally applied driving voltage U can be reduced by generating a stationary standing wave field in the sample with overtone adjusted transmitting transducers.

The threshold density of acoustic energy flux w_{th} for the occurrence of SL is approximately one to several W/cm^2 in CdS samples but is considerably higher, of the order of 10 W/cm^2, in alkali halides (Ostrovskii, 1981). From these values, important information is obtained on the range of compression and accompanying disturbances of the materials exhibiting SL effect. For example, in the MHz frequency range employed in the SL studies presented here, the typical ionic displacements are rather small. They can roughly be estimated from the relation

$$a_0 = (1/2\pi f)(2w_{th}/\rho v)^{1/2}\,. \tag{1}$$

Using a threshold acoustic intensity w_{th} of 1 W/cm^2 in CdS crystals, one obtains $a_0 \sim 0.8$ nm by choosing a frequency $f = 10$ MHz, a lattice density $\rho = 4.8$ g/cm^3 and by implicitly assuming pure shear waves of velocity $v = 1.75 \times 10^3$ m/s (McFee, 1966). The resulting acoustic strains,

$$s_0 = (2\pi f a_0/v)\,, \tag{2}$$

amount to about 3×10^{-5} and, hence, do not exceed the elastic limit for static strains in CdS crystals. However, they are sufficiently high to drive dislocations away from their equilibrium positions and thus may yield inelasticity effects (Ostrovskii and Lysenko, 1984).

One way of demonstrating the appearance of a dislocation inelasticity is, for example, to discuss this matter in terms of electromechanical coupling or mechanical quality factors. Thus far, the piezoelectric coupling between elastic and electric energy has been shown to change due to point defects and dislocations (Chubachi et al., 1971). In order to attain these factors, the resonance–antiresonance method is frequently used (see, for example, Mason, 1964). By employing the driving frequency-dependent mechanical vibrations of CdS platelets, the electromechanical coupling factor K and the mechanical quality factor Q can readily be calculated from the following relations:

$$K^2 = (\pi/2)(f_r/f_a)\mathrm{tg}(\pi(f_r - f_a)/2f_a)\,, \tag{3}$$

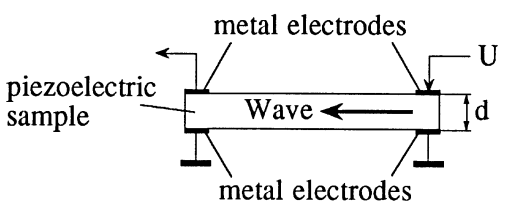

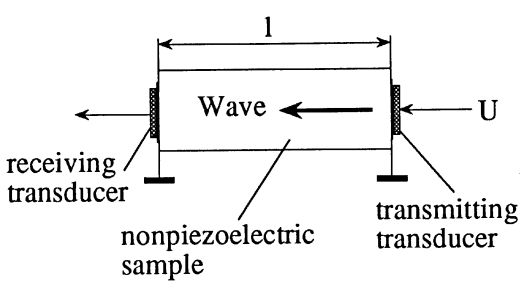

Fig. 1. Schematic drawing of the experimental setup for SL production in piezoelectric crystals. The thickness d of the plate ranges from a few dozens to a few hundreds μm.

Fig. 2. Experimental setup for measuring SL in nonpiezoelectric crystals. The length l of the sample ranges from about 3 to 30 mm.

and

$$Q = f_r/\Delta f, \tag{4}$$

where f_r and f_a are the resonance and antiresonance frequency of the sample admittance, respectively, and Δf is the width of the curve displaying the frequency dependence of the sample admittance taken at 0.707 of its maximum value.

Measurements of the K and Q factors exemplified in Fig. 3 demonstrate the existence of a rapid decrease in the electromechanical coupling and mechanical quality factors for driving amplitudes above the threshold value U_{th} for the occurrence of SL. These drops have been understood largely in terms of enhanced defect concentrations exerted by the above-threshold drivings (Ostrovskii and Lysenko, 1984).

Today, a large set of data is available signifying an unambiguous correlation between dislocation densities in the samples and the occurrence of SL (Ostrovskii and Korotchenkov, 1981, 1985; Ostrovskii and Lysenko, 1984). This correlation is most strikingly characterized by comparing changes in the SL intensity with the evolution of the density of dislocation pits due to chemical etching of cleaved facets in NaCl with increasing driving amplitude. Despite intense scrutiny, studies of acoustically driven samples with etch-pit techniques are rarely reported (see, for example, Tyapunina et al., 1982, 1988). Fig. 4 shows the dependence of the integrated SL intensity on the driving amplitude which reveals two pronounced regions with different slopes marked by ab and bc. The rapid increase in the SL intensity above point b can most probably be related to an enhanced dislocation density due to the multiplication of dislocations as shown in Fig. 5. Indeed, no evidence of an increased pit density is seen in Fig. 5a taken in the re-etched sample after driving in the amplitude range ab in Fig. 4. However, a further increase in the driving amplitude just above

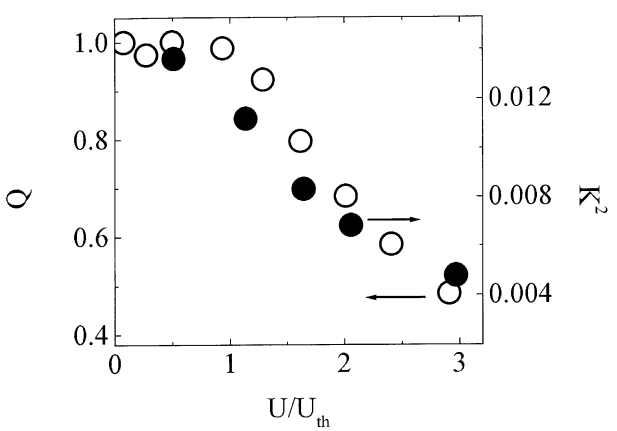

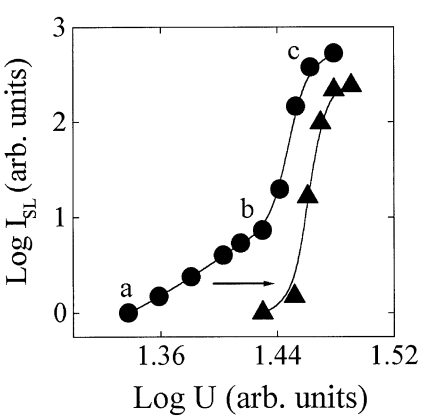

Fig. 3. Electromechanical coupling factor K and mechanical quality factor Q versus the amplitude of acoustic driving in a CdS platelet. The threshold driving amplitude U_{th} corresponds to the appearance of the SL effect in the platelet. After Ostrovskii and Lysenko (1984).

Fig. 4. Intensity of the room-temperature SL versus the driving amplitude at $f \sim 2$ MHz in a NaCl sample. The data labeled by circles were taken in a sample initially loaded with the driving whereas the data labeled by triangles represent the run taken in a sample preexposed to about 15 min driving with the amplitude close to point c.

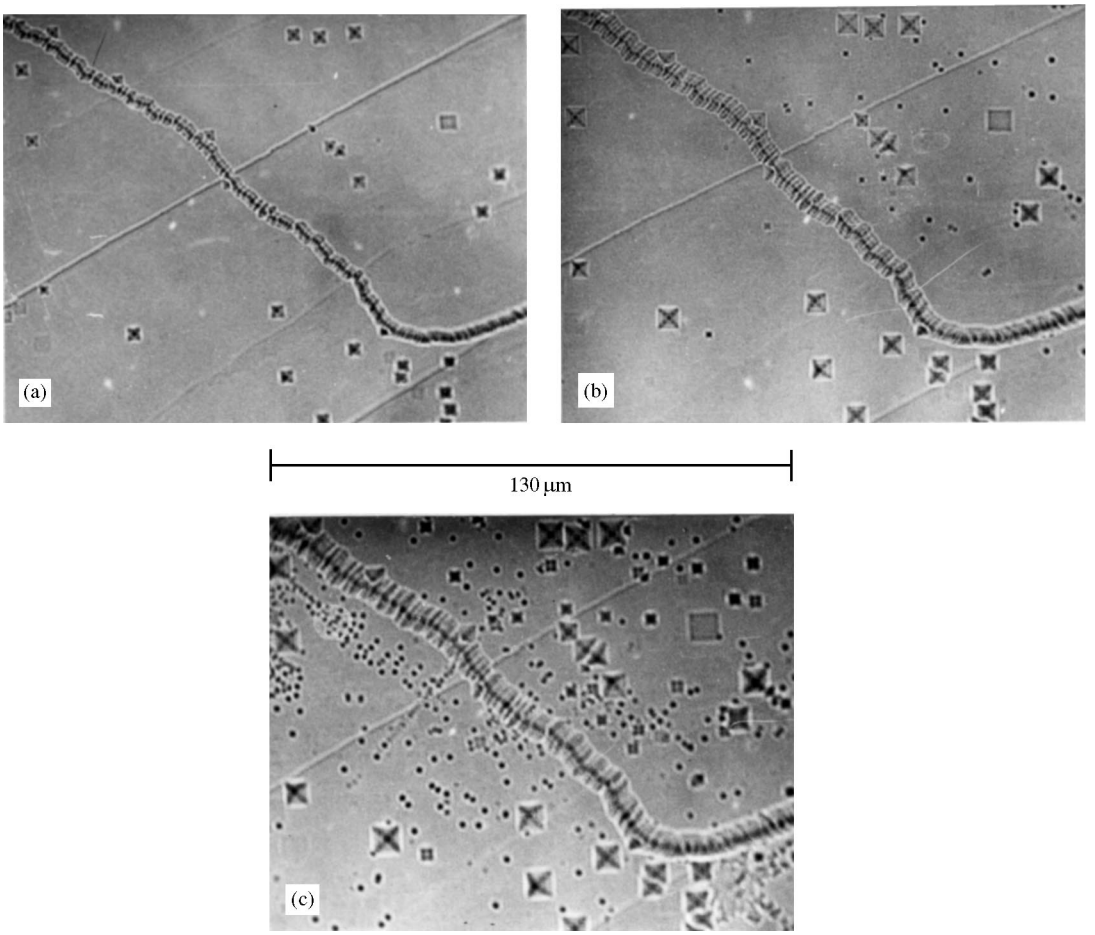

Fig. 5. Representative microphotographs of dislocation etch pits developed on a cleaved surface of NaCl subjected to driving in the amplitude region ab in Fig. 4a, and close to the point b of the region bc in Fig. 4b and Fig. 4c. The time of preexposure to the driving at the given amplitude is 5 min for the microphotographs a and b, and 10 min for c.

point b in Fig. 4 leads to additional dislocation pits implying that the density of the surface-terminated dislocations increases with the driving time (microphotographs b and c in Fig. 5). One also observes that the threshold amplitude for the occurrence of SL becomes larger and the initial region ab of the SL increase in Fig. 4 tends to decrease (triangles in Fig. 4) with increasing density of dislocations.

All these examples suggest that the defect-mediated mechanism may indeed provide a sound understanding of such sonoluminescence phenomenon.

3.2. Light-emitting mechanism

It seems to be difficult to describe the appearance of SL in the frameworks of electroluminescence or deformation luminescence mechanisms (Lysenko and Ostrovskii, 1981a; Ostrovskii and

Lysenko, 1981). Using piezoelectric CdS plates as a convenient reference, the threshold intensity w_{th} for observing SL corresponds to an externally applied electric field strength U_{th}/d of the order of 5 kV/cm in the experimental setup exhibited in Fig. 1. Near the plate resonances, this value increases by a factor which depends on the mechanical quality factor of the plate. This is not surprising considering that the strength of the piezoelectric field F_{piezo} accompanying thickness vibrations of a piezoelectric resonator is given by (Lysenko and Ostrovskii, 1981a)

$$F_{piezo}(f,x) = (U/d)\{[(\cos(\pi fd/v) - K^2\cos(2\pi fx/v)]^2 + \pi^2/16Q^2\}^{1/2} \times \{[(\cos(\pi fd/v) - (vK^2/\pi fd)\sin(\pi fd/v)]^2 + \pi^2/16Q^2\}^{-1/2}, \quad (5)$$

with $x = \pm d/2$ being the coordinates of the surfaces of a vibrating platelet. It is readily seen that the maximum field is achieved at the resonance frequency f_r defined by

$$\cos(\pi f_r d/v) = (vK^2/\pi f_r d)\sin(\pi f_r d/v). \quad (6)$$

Hence, the strength of the piezoelectric field at the resonance frequency f_r is of the form

$$F_{piezo}(f_r,x) = (U/d)\{1 + (16Q^2K^4/\pi^2)[\sin(\pi f_r d/v)/(\pi f_r d/v) - \cos(2\pi f_r x/v)]^2\}^{1/2}. \quad (7)$$

Taking $Q = 50$ and $K = 0.19$ as typical values in CdS, an upper limit for the threshold strength of the piezoelectric field is about 11 kV/cm. According to Lysenko and Ostrovskii (1981a), CdS plates cannot maintain electroluminescence effects at such high externally applied electric fields. It is therefore most probable that the piezoelectric fields accompanying the driving are too low to describe the SL phenomenon in the framework of electroluminescence mechanisms.

The distribution of the mechanical displacement $a(f,x)$ inside the vibrating plate is approximated by (Ostrovskii and Lysenko, 1981)

$$a(f,x) = (eU/2\pi\rho vfd)\sin(2\pi fx/v)\{[(\cos(\pi fd/v) - (vK^2/\pi fd)\sin(\pi fd/v)]^2 + \pi^2/16Q^2\}^{-1/2}, \quad (8)$$

where e is the piezoelectric constant and ρ is the density of the sample. Eqs. (5) and (8) provide important information because they deal with very different frequency dependencies of the piezoelectric field and mechanical displacement.

It may therefore be helpful to compare the frequency dependence of the integrated SL intensity and the sample admittance which are shown in Fig. 6. While the admittance exhibits a maximum and a minimum at frequencies f_r and f_a, respectively, (downward arrows in Fig. 6) the sonoluminescence intensity peaks between f_r and f_a. This observation suggests that the occurrence of SL should be related to mechanical vibrations rather than piezoelectric fields (Ostrovskii and Lysenko, 1981).

At this point, it is worth noting that extensive work on mechanically induced luminescence has been performed for decades in a large variety of materials (Bredikhin and Shmurak, 1979; Poletaev and Shmurak, 1984; Walton, 1977; Chandra et al., 1990; Zakrevskii and Shuldiner, 1995). Mechanoluminescence has been observed by compressing, scratching, cleaving, shaking, grinding, and crushing of solids. In II–VI compounds, for example, it is widely accepted that the movement of charged dislocations is the predominant process for the transfer of initial mechanical excitation into light. Part of the mechanoluminescence, however, is likely to be due to the deformation-induced direct excitation of luminescence centers.

Within the framework of dislocation models, the transfer of mechanical excitation into light can occur by three different channels. Firstly, electrons captured at trapping centers are excited into the

conduction band due to the electrostatic interaction with moving charged dislocations. Subsequent recombination of free electrons with holes bound to the luminescence centers produces stationary light emission. Secondly, movement of charged dislocations towards a crystal surface gives rise to flashes of light because of electrical breakdowns occurring at the surface. Thirdly, it has been suggested that electrons or holes can be transferred to dislocation energy bands where they recombine radiatively with free holes or electrons.

Although the physics behind the nature of SL could qualitatively be similar to that explaining deformation luminescence effects, the physical models describing the occurrence of SL cannot simply be treated in terms of external electric fields or (quasi)static compressions. In order to satisfy all the experimentally observed properties of SL, a model of sonoluminescence has been developed by Ostrovskii (1981). It claims that the dislocation motions driven by a sufficiently intense acoustic field produce vacancy – interstitial pairs of the host atoms which disappear after the removal of the acoustic driving. Radiative transitions within the defect pairs are then responsible for the observed SL. Although a large number of papers on this topic has been published later, this model of SL seem yet to be valid. The SL concept is simple, but detailed information about the atomic-scale picture of the processes is so far still lacking implying that little progress has been made towards a satisfactory theoretical description. There are still many open questions concerning the detailed theory of this phenomenon.

To improve our understanding of SL, it may be helpful to take a closer look on sonoluminescence spectra. As shown in Fig. 7, SL spectra of CdS platelets display a variety of prominent bands typically observed in photoluminescence (PL) studies. The peak at about 515 nm is a well-known green donor–acceptor pair band (Colbow, 1966) accompanied by LO phonon replicas on the long-wavelength side of the SL spectrum. This band is generally attributed to a donor level 0.03 eV below the conduction band and an acceptor level 0.17 eV above the valence band. This implies that the interstitial sulfur S_i^- and the cadmium Cd_i^+ atoms are most probably involved in the green SL band (Ostrovskii, 1981).

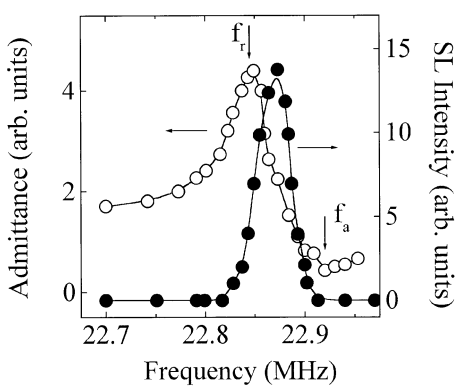

Fig. 6. Frequency dependence of the admittance (open circles) and the integrated SL intensity (closed circles) in a CdS platelet at 77 K. From Ostrovskii and Lysenko (1981).

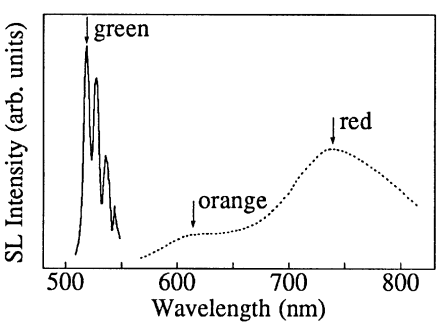

Fig. 7. Typical low-temperature SL spectra observed in CdS platelets showing green (solid curve), orange and red (dashed curve) emission bands. The dashed spectrum is taken from Ostrovskii (1981).

The broadband at about 605 nm (Fig. 7) is an orange luminescence band of CdS which is observed in the range between 595 and 605 nm in undoped CdS samples. Since the earliest studies of Kulp (1962), it is assumed that this band originates from cadmium interstitial atoms Cd_i but further and still more detailed studies on which luminescence center is indeed involved have been and will be performed (Mochizuki et al., 1983; Krustok, 1992). It has, for example, been observed that the emission intensity of the orange band increases with increasing partial pressure of cadmium in thermally treated samples. As such a treatment is generally believed to increase the concentration of cadmium interstitials or sulfur vacancies, it is therefore likely that these intrinsic defects are related to the origin of the orange emission band (Mochizuki et al., 1983). Indeed, it has been shown that the orange emission band observed in SL spectra is most probably due to the recombination of a free hole with an electron trapped at a defect complex consisting of interstitial cadmium Cd_i^+ and sulfur vacancy V_S^+ atoms (Ostrovskii and Rozhko, 1985).

The red emission band also seen in Fig. 7 at about 740 nm is related to the sulfur vacancies (Kulp and Kelley, 1960). It is currently believed that the red SL arises from associated donor–acceptor pairs of sulfur and cadmium vacancies (V_S^+, V_{Cd}^-) (Ostrovskii, 1981).

The question arises now whether or not the involvement of defects in the SL spectra really proves the generation of defects due to acoustic driving. Mechanical excitation of luminescence centers which are already present in the crystals could likewise explain most of the spectroscopic results. The majority of the data, however, obtained in a variety of studies clearly indicates that, in the driving range used, it is the displacement of atoms from their lattice sites due to acoustically driven motions of dislocations that produces nearest-neighbor pairs of opposite signs and that these pairs act as sonoluminescence centers. Some results in this context are worth to be mentioned in more detail.

3.2.1. Acoustically driven generation of point defects

SL spectra show emission peaks which are absent in photoluminescence spectra of the same samples and similar bands as the one detected in SL have been observed in acoustically driven PL (Ostrovskii and Korotchenkov, 1985, 1992). This is clearly seen in Fig. 8 which exhibits both spectra of PL as well as the ones of acoustically driven PL (ADPL) and SL all taken in a ZnS crystal. The photoluminescence spectrum presented in Fig. 8 shows a weak green emission band at about 520 nm the origin of which is still unclear. Several different models have been attempted to explain the emission. Rizakhanov et al. (1978), for example, used a unified model which builds upon the blue self-activated emission (Samelson and Lempicki, 1962) and the green emission bands. These bands have been ascribed to radiative transitions of free carriers into associated pairs of spatially separated charged defects. They have been quantitatively explained by using a simple theory and assuming that the Coulomb approximation of interacting defects can be applied. On the other hand, Georgobiani et al. (1983) have argued that the green emission band at about 520 nm shows evidence of a single peak which can be explained by a radiative recombination process involving free electrons and doubly charged sulfur vacancies V_S^{++}.

In contrast to the PL spectrum, the ADPL spectrum of Fig. 8 shows an enhanced emission band with a complicated structure in the green part of the spectrum. Interestingly, similar, but still more pronounced peaks are exhibited in Fig. 8 by the SL spectrum. Based on these observations, it has been suggested already previously that the observed structure of the green emission must originate from radiative recombinations between free electrons and holes trapped at deep donors V_{Zn}^- (zinc vacancy) in the Coulomb field of singly charged acceptors A_k on cation sites (Ostrovskii and

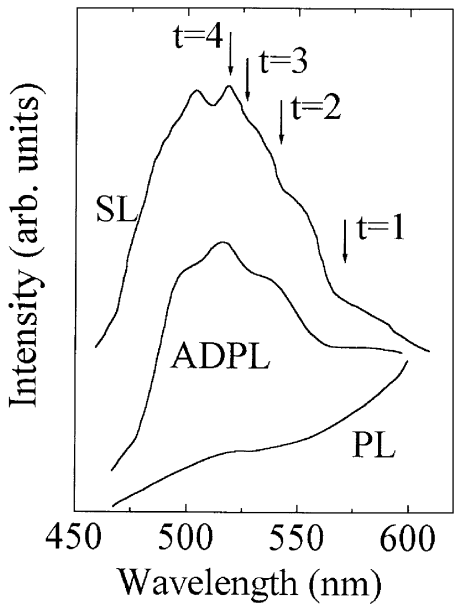

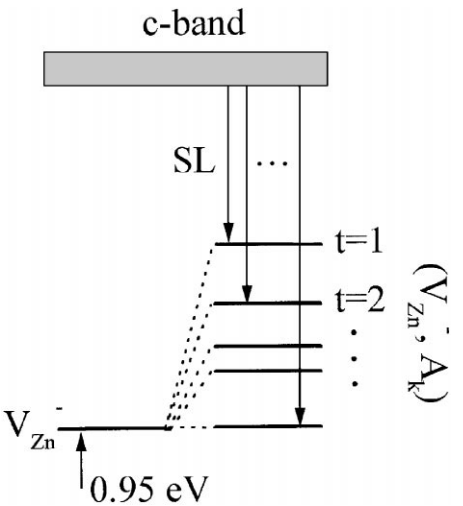

Fig. 8. Typical room-temperature photoluminescence (PL), acoustically driven PL (ADPL) and sonoluminescence (SL) curves obtained with a cubic ZnS : Ag (10^{-2} at%) sample. The PL and ADPL spectra are taken from Ostrovskii and Korotchenkov (1992).

Fig. 9. Suggested energy level scheme for the ADPL and SL multiple peak structure shown in Fig. 8. The levels are calculated from Eq. (9) using $r_1 = 3.83$ Å, $r_2 = 5.41$ Å, $r_3 = 6.63$ Å and $r_4 = 7.66$ Å derived from the lattice structure parameters.

Korotchenkov, 1985, 1992). The energy levels (V_{Zn}^-, A_k) obtained from such a model (Fig. 9) are readily calculated from

$$E_t = E(V_{Zn}^-) + e_0^2/4\pi\varepsilon_0\varepsilon r_t\,, \tag{9}$$

where $E(V_{Zn}^-) = 0.95$ eV is the energy depth of a zinc vacancy (Georgobiani et al., 1983), r_t is the spatial separation between V_{Zn}^- and A_k, and e_0 is the electron charge. The other symbols have their usual meaning.

Since V_{Zn}^- and A_k occupy lattice sites, only certain values of r_t are permitted and discrete peaks are therefore expected in acoustically driven spectra. Considering that $E_g = 3.68$ eV and $\varepsilon = 8.3$ in ZnS, the electronic transitions between states in the conduction band and the (V_{Zn}^-, A_k) deep center are expected to be in the wavelength region between about 470 nm ($r_t \to \infty$) and 570 nm ($r_t = r_1$) which is fully consistent with the ADPL and SL bands presented in Fig. 8. As already mentioned, this model also accounts for the appearance of a multiple peak structure in the ADPL and SL spectra as evidenced by arrows in Fig. 8 indicating the calculated wavelengths.

In developing the model of SL further, it may be helpful to emphasize once again the pronounced drop of the electromechanical coupling factor and the mechanical quality factor accompanying the occurrence of SL in CdS resonators (Fig. 3). In this respect, it is worth mentioning that the coupling

factor between electrical and elastic energy has been shown to decrease considerably with increasing defect concentrations (Wilson, 1966; Chubachi et al., 1971).

It has further been observed that the intensities of the bound exciton PL lines in CdS increase when the sample is exposed to above-threshold acoustic fields which is considered as an indication for enhanced concentrations of point defects (Ostrovskii and Lysenko, 1982). This is clearly seen in Fig. 10 which shows that the I_2 and I_3 emission lines associated with excitons bound to neutral and ionized donors, respectively (Thomas and Hopfield, 1962), are considerably enhanced after exposing the CdS platelet to above-threshold acoustic driving. It is also seen that (a) the PL intensities are suppressed when the driving is switched on (curves 2 and 4 in Fig. 10), whereas they increase when the driving is switched off (curves 1 and 3 in Fig. 10) and that (b) the enhancement of the I_3 emission line associated with an ionized donor (curve 3 in Fig. 10) is much larger than the one of the I_2 line which is due to a neutral acceptor (curve 1 in Fig. 10). The I_2 emission line obviously decreases at the largest driving amplitudes employed (at $U \geq 1.5$ V). Finally, the enhancement of the exciton emissions is still observed several minutes after the removal of the driving, and is found to disappear completely first after more than 20 min.

Presently, it seems that the presence of neutral and ionized local centers binding excitons is best understood in terms of acoustically driven defect generation and ionization processes. In order to check this model in more detail, the excitonic structure of acoustically driven photoconductivity (PC) has been studied in CdS plates, as will be discussed later.

3.2.2. Sonoluminescence and dislocations

As mentioned above, evidence for a dislocation mediation of the SL effect is supported by experiments involving chemical etching which increases the number of etch pits on the crystal surface (Ostrovskii and Korotchenkov, 1981; Ostrovskii and Lysenko, 1984). Furthermore, there is a predictive correlation between SL and the generation of acoustic emissions originating from dislocation motions (Kalitenko et al., 1985).

During deformation of solids, strain energy is violently released as vibrations or sound waves; this phenomenon is known as acoustic emission (AE) (Joffe, 1928; Lord, 1975). Among various mechanisms of AE sources, current experimental evidence strongly supports models which explain bursts of AE in terms of a sudden rush of dislocations. It has long been recognized that the AE pulse rate is proportional to the time rate of the change in a mobile dislocation density, particularly, in single crystals of NaCl and LiF (James and Carpenter, 1971). It has also been reported that AE results in metals correlate better with changes in dislocation motions occurred by breakaway from pinning points than with changes in the total dislocation density (Jaffrey, 1979). Therefore, since the acoustic emission pulse rate would be expected to follow closely the acoustically driven dislocation movements, comparative studies of SL and AE effects have been set forth by Kalitenko et al. (1985).

The correlation of SL and AE events is most conveniently monitored by the setup presented in the inset of Fig. 11. The presented unit employs a single crystal of NaCl (1), transducer (2) typically driven at frequencies of 2–7 MHz, and a detector (3) of AE. The AE signal is sensed by a resonant piezoelectric transducer with a thickness resonance frequency of about 200 kHz being fed into a pass-band filter and a threshold counter of AE pulses.

Fig. 11 shows the AE pulse rate (open circles) and the SL intensity (filled circles) versus the driving amplitude. As one can see, the AE pulses begin, within the experimental resolution, at the

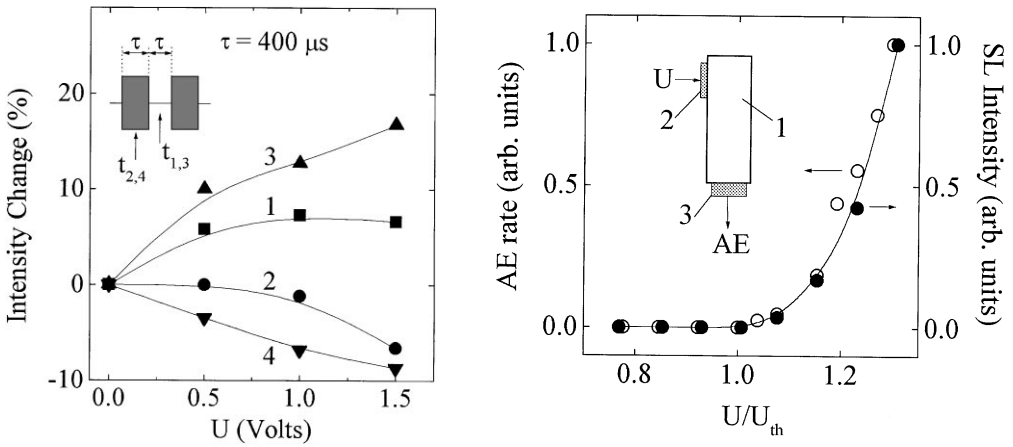

Fig. 10. Intensities changes of the I_2 (curves 1 and 2) and I_3 (curves 3 and 4) exciton PL line in CdS taken at 4.2 K with (curves 2 and 4) and after (curves 1 and 3) applying the above-threshold acoustic driving. The inset illustrates the experimental setup: the driving is performed by acoustic tonebursts (shadow patterns), the PL intensities are taken at times $t_{2,4}$ and $t_{1,3}$. The average acoustic power is about 1 W/cm^2 for the maximum driving amplitude. From Ostrovskii and Lysenko (1982).

Fig. 11. AE rate (open circles) and SL intensity (filled circles) as a function of the driving amplitude in a NaCl crystal at room temperature. Both curves are normalized to their maximum value. The inset shows the experimental setup with a NaCl sample (1), a 3.75 MHz-driven piezoelectric transducer (2) and a detector for the AE signal (3). From Kalitenko et al. (1985).

same driving amplitude which yields the sonoluminescence effect. The AE rate increases rapidly above the threshold driving amplitude. Interestingly, two types of acoustic emission have been detected over the range of the driving amplitude used, though no particular models have yet been developed to distinguish between them. The emission has been found to initially arise as a burst-type signal which is followed by a continuous or high-frequency type upon further increasing the driving amplitude.

Although quite a bit is known about acoustic emission in mechanically deformed solids, little consideration has been given to the emission processes at acoustic drivings. Based on precise etch pit measurements, Kalitenko et al. (1987) argued that the AE pulses must be related to the kinetics of dislocation motions. This finding had some implications on an appropriate study performed by James and Carpenter (1971) at constant compressive deformation. Their study demonstrated that the AE pulse rate cannot in a straightforward manner be related to the change of the total dislocation density due to dislocation multiplication or to the density of mobile dislocations. This is in agreement with the results exhibited in Figs. 11 and 5a which indeed indicate a complete lack of correlation between the occurrence of acoustic emission and the multiplication of dislocations at $U \approx U_{th}$. Hence, the experimental data seem to be best described by implying the AE rate to be proportional to the rate of the change of the mobile dislocation density originating from (i) dislocation breakaway from pinning points, and (ii) the creation of mobile dislocation lines by multiplication. It should be stressed, however, that this seems to be an issue that will need further consideration.

Another example regarding the dislocation mediation of SL is the dislocation damping effect which is observed by employing a cw acoustic beam and a probe toneburst acoustic beam for generating SL (Ostrovskii and Korotchenkov, 1988). In these experiments, the attenuation α of the probe beam has been determined by a standard echo-pulse technique (Truell et al., 1969) which measures the amplitude of the exponentially decaying reflected pulses traveling across the sample. The change in the attenuation of the probe beam has been detected by increasing the cw driving amplitude.

Changes of α and the SL intensity as a function of the driving amplitude are presented in Fig. 12. The appearance of SL at $U \geq U_{\text{th}}$ in Fig. 12a is accompanied by a rapid increase of the acoustic attenuation (filled circles in Fig. 12b). Further, the acoustic loss at $U \geq U_{\text{th}}$ exhibits a hysteresis loop (open circles in Fig. 12b) which is not observed at $U < U_{\text{th}}$ and implies the participation of dislocations.

An interesting approach to acoustically driven dislocation dynamics is introduced by Burlak and Ostrovskii (1997). The authors start from the wave equation (Einstein summation of repeated indices)

$$\rho(\partial^2 u_i/\partial t^2) = (\partial S_{ik}/\partial x_k) \,. \tag{10}$$

The motion of dislocation loops is approximated by the vibrating string model of dislocations developed by Granato and Lücke (1956a,b) as

$$A(\partial^2 \zeta_i/\partial t^2) + B(\partial \zeta_i/\partial t) = f_i \,, \tag{11}$$

where u_i are the components of the wave displacement vector (particle displacements), S_{ik} are the stress tensor components, x_k are Cartesian coordinates, and ζ_i are the components of the dislocation loop displacement vector, A is the effective mass of a dislocation per unit length, B is the dislocation damping parameter per unit length, and f_i are the components of the external force per unit length exerted on dislocations. It is convenient to write S_{ik} and f_i in the form

$$S_{ik} = (\partial \Phi/\partial T_{ik}), \quad f_i = -(\partial \Phi/\partial \zeta_i) \,, \tag{12}$$

where T_{ik} are the components of the strain tensor. The free energy Φ of the system can be expressed in terms of T_{ik} and ζ_i as

$$\Phi = (1/2)\lambda_{ijkl} T_{ij} T_{kl} + (1/2) C_{ik} \zeta_i \zeta_k + (1/2)\beta_{ijkl}(b_i \zeta_j + b_j \zeta_i) T_{ik} \,, \tag{13}$$

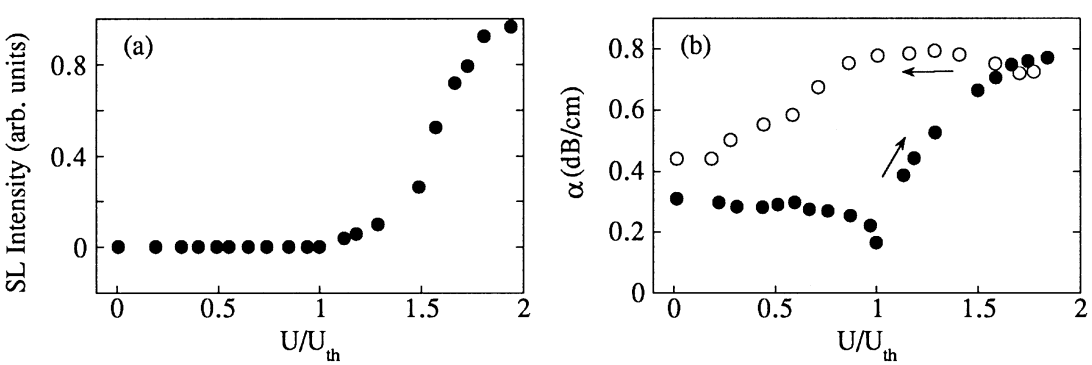

Fig. 12. Integrated SL intensity (a) and acoustic attenuation (b) versus the amplitude of acoustic driving in ZnS : Ag. The filled circles were taken for increasing driving amplitude while the open circles were measured for decreasing amplitudes.

λ_{ijkl} being the elastic coefficients, C_{ik} the dislocation tension parameters, β_{ijkl} the tensor of acoustodislocation interaction and b_i the Burgers vector components.

In a pioneering approach, Burlak and Ostrovskii (1997) described the dislocation nonlinearity in acoustic fields by expanding the dislocation effective mass A, tension C and damping parameter B of dislocations in terms of the dislocation displacement $\zeta(\zeta_i = \zeta, T_{ik} = T, i, k = 1)$

$$A = A_0(1 + A_1\zeta^2), \quad C = C_0(1 + C_1\zeta^2), \quad B = B_0(1 + B_1\zeta^2 + B_3\zeta^4 + B_2\Delta l^2) \,. \tag{14}$$

Here, A_i, B_i and C_i are constant coefficients, and Δl^2 is the average dislocation loop defined as

$$\Delta l^2 = \chi\,\zeta^2\Theta(\zeta^2 - \zeta_c^2)\int_0^x T^2\,\mathrm{d}x \,, \tag{15}$$

The parameter $\Theta(\zeta^2 - \zeta_c^2)$ is the step function such that

$$\Theta(\varsigma^2 - \varsigma_c^2) = \begin{cases} 0 & \text{if } |\varsigma| < |\varsigma_c| \,, \\ 1 & \text{if } |\varsigma| \geq |\varsigma_c| \,, \end{cases} \tag{16}$$

is equal to zero at low driving amplitudes and to unity when the dislocation displacement exceeds some critical value ζ_c. This critical value corresponds to the generation of lattice defects in acoustic fields attained at the particle displacement amplitude u_c which is close to the lattice constant. Solving Eqs. (10) and (11) by the method of slowly varying amplitudes, the complex amplitude $u_0(x, t)$ of the acoustic wave has been found to satisfy the equation

$$(\partial/\partial t + v(\partial/\partial x))u_0 = -\left[\gamma - a_2\left(1 - \chi\Theta(u_0^2 - u_c^2)\int_0^x u_0^2\,\mathrm{d}x\right)u_0^2 + a_3u_0^4\right]u_0 \,, \tag{17}$$

where γ is the phenomenological parameter of an acoustic attenuation and a_2 and a_3 are coefficients. It should be mentioned that, at low driving amplitudes, Eq. (17) describes the propagation of the toneburst acoustic beam with attenuation γ. At higher drivings, however, Eq. (17) becomes nonlinear with the attenuation depending on the driving amplitude.

Eq. (17) can only be solved numerically. The result of such a numerical simulation is shown in Fig. 13. The good agreement between theory and experiment is exhibited by comparing Fig. 13 and Fig. 12b. It is seen that theory predicts a hysteresis loop in acoustic losses at $U \geq U_{th}$, and this behavior is experimentally observed in Fig. 12b. Moreover, the acoustic loss presented in Fig. 12b shows a pronounced drop at subthreshold drivings $U \leq U_{th}$. Analyzing the simulated curve displayed in Fig. 13, it is readily seen that such a behavior is surprisingly well predicted by the theory outlined here, in marked contrast with the string model of Granato and Lücke (1956a,b) and its modifications (see, for example, Swartz and Weertman, 1961). One may therefore conclude that dislocations are obviously linked to the observed production of light in SL phenomena.

3.3. *Acoustically driven defect charges and related effects*

In this section, we would like to demonstrate that moving charged dislocations and charges at point defects due to acoustic driving may cause significant effects on optical spectra. The field strengths in a solid containing charged point defects is approximated by the normal field

$$F_0 = e_0/4\pi\varepsilon_0\varepsilon r_0^2 \,, \tag{18}$$

in terms of the nearest ion distribution (Redfield, 1963). Here, $(4\pi/3)r_0^3 = 1/N$ is the mean volume per defect and N is the defect concentration. Taking $\varepsilon = 9$ for a CdS crystal and $N \sim 10^{17}\ \mathrm{cm}^{-3}$ which may be considered as a reasonable approximation for an easily measurable intensity in SL, one obtains $F_0 \sim 9 \times 10^3$ V/cm.

Charged dislocations in semiconductors are often treated as noninteracting space-charge regions with electric fields being shielded by free carriers. However, as dislocations move in externally applied fields they acquire a charge (Petrenko and Whitworth, 1980; Whitworth, 1985) implying that considerable electric fields may occur. In the case of acoustically driven CdS crystals, dislocation field strengths in excess of 3×10^4 V/cm have been reported (Ostrovskii and Das, 1997).

3.3.1. *Acoustically driven optical absorption edges*

This analysis clearly indicates that acoustically driven samples are pervaded by electric fields of considerable strengths. Standard lore tells us that these fields should obscure the normally observed flatness of the energy band diagram and cause a shift of the fundamental optical absorption edge, as originally pointed out by Redfield (1963). This effect is indeed observed when analyzing the data exhibited in Fig. 14. The low-energy shift of the transmission edge (T_U compared to T_0 in Fig. 14) which amounts to about 50 meV, exceeds quite remarkably the 11 meV expected from the A-exciton reflectance line (R_U compared to R_0). It should be noted that the energy of the A-exciton reflectance peak associated with the Γ_9 valence band (Thomas and Hopfield, 1959) is given by

$$E_A = E_g - E_B\,, \tag{19}$$

where E_g is the band gap energy and E_B is the binding energy of the exciton. The binding energy E_B is assumed to be nearly undisturbed by the driving since there is currently no other experimental

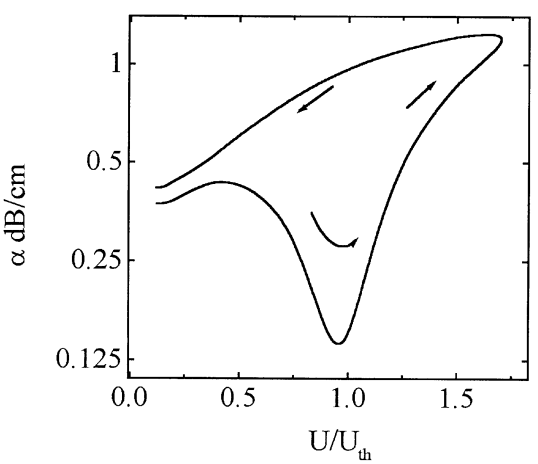

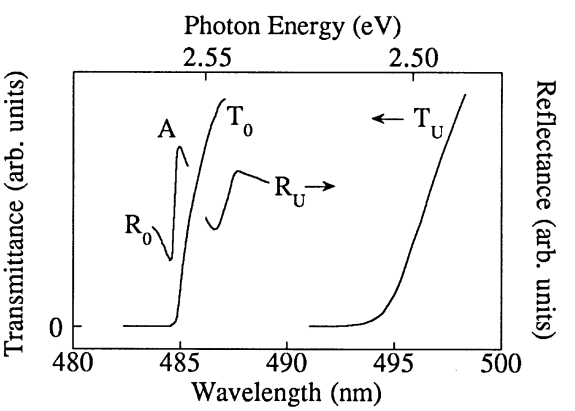

Fig. 13. Numerical simulation of the acoustic attenuation versus driving amplitude (Eq. (17)) at $a_2 = -0.05$, $a_3 = 0.3$, $\gamma = 0.47$. From Burlak and Ostrovskii (1997).

Fig. 14. Reflectance (A-exciton line) and transmission spectra of a CdS platelet at 4.2 K at $U = 0$ (R_0 and T_0, respectively) and $U = 1.2\ U_{th}$ (R_U and T_U) experiencing acoustically driven low-energy shifts. From Ostrovskii (1981).

evidence. The shift of the reflectance line seen in Fig. 14 illustrates most likely the shift of E_g to lower energies due to the internal electric field generated by the acoustic driving and, hence, is the analogy of the Franz–Keldysh effect observed with external electric fields. The shift therefore reflects the degree by which the band edges are blurred because of the field. If it is further assumed that the shift $\delta E_g = 11$ meV deduced from Fig. 14 is due to charged point defects which are produced by the driving, the defect concentration N is readily calculated by fitting δE_g to the equation often used to describe the Franz–Keldysh effect (e.g., Pankove, 1975)

$$\delta E_g = (3/2m^{*1/3})(e_0\hbar F_0)^{2/3} . \tag{20}$$

Here, $m^* = 0.141m_0$ (Wang et al., 1990) is the reduced interband effective mass whereas the other symbols have their usual meaning. The fitting gives a value of 10^4 V/cm for the normal field F_0 which suggests an upper limit of 1.2×10^{17} cm^{-3} for the defect concentration N according to Eq. (18). As mentioned earlier, this seems to be a reasonable estimate.

The enhanced shift of the transmission edge in comparison with the reflectance line (Fig. 14) has been interpreted as an analogy to the impurity absorption process (Ostrovskii, 1981). As may be expected, electronic transitions at shallow defect states which are produced by the driving may mingle with electronic interband transitions resulting in a misleading discrepancy between the low-energy shifts of the reflectance and transmission spectra. This interpretation is in agreement with the reported value for the binding energy of the cadmium interstitials which is (0.06 ± 0.03) eV (Ermolovich et al., 1977) and obviously accounts for the energy difference of about 40 meV between the optical reflectance and transmission spectra (Fig. 14). These observations provide further evidence for the underlying defect generation process.

3.3.2. Acoustically driven photoconductivity

Additional evidence of the defect generation process is obtained from experiments involving acoustically driven photoconductivity. Measurements on CdS platelets demonstrate the remarkable redistribution of PC peaks with acoustic drivings and the appearance of lines which may originate from excitons trapped by certain centers. Spectrum 1 in Fig. 15, for example, is a low-temperature photoconductivity spectrum of an as-grown CdS platelet. It is well documented that three intrinsic exciton series exist in CdS, the A-, B- and C-series, arising from electrons in the conduction band, and holes in each one of the triply degenerated valence bands (Hopfield and Thomas, 1961). Absorption of light at the exciton energies is known to lead to the formation of excitons which in part may dissociate into free carriers and thus appear as peaks in the photoconductivity spectra. Hence, the bands marked by arrows A and B in Fig. 15 are believed to be due to free carriers from dissociated intrinsic excitons A and B, respectively, as pointed out by Ostrovskii and Rozhko, 1984. The authors found that the above-threshold acoustic driving produces a redistribution of the PC bands and the appearance of a set of new PC peaks. In particular, curve 2 in Fig. 15, taken after the crystal has been exposed to the driving, shows a short-wavelength band which peaks at about 480 nm in addition to several new peaks on the long-wavelength side of the A- and B-exciton bands.

The dominant contribution to the long-wavelength peaks are likely to originate from A and B excitons trapped by a neutral donor. It is therefore most likely, that the bound exciton I_2 derived from the A exciton and with an energy of 6.6 meV below the A exciton (Thomas and Hopfield, 1962), is predominantly responsible for the band seen at about 487 nm in spectrum 2 of Fig. 15. It

should be noted, however, that several other lines associated with exciton complexes are usually observed in this region (Thomas and Hopfield, 1962; Reynolds and Litton, 1963). The overlap of some of these lines may therefore give rise to a more complex structure of the band at about 487 nm as indicated by the data presented in Fig. 15.

The 483 nm line seen in spectrum 2 of Fig. 15 is separated from exciton B by approximately the same energy (about 6.1 meV below the B exciton) as the I_2 line is from exciton A. It seems therefore reasonable to assume that the line at about 483 nm arises from the bound exciton I_{2B} in the notations of Thomas and Hopfield (1962).

The assignment of the short-wavelength band at about 480 nm is not straightforward. However, there are several arguments concerning the most reasonable choice for the interpretation of this band. The I_2 exciton line at 486.7 nm and the band at about 480 nm exhibit an energy difference of about 37 meV which is close to the LO phonon energy $\hbar\omega_{LO} = 37.7$ meV in CdS (Langer et al., 1966). It has already been pointed out previously by Langer et al. (1966) that photons with the energy of an exciton and an LO phonon appear to cause a minimum in the photocurrent because the fraction of such excitons which annihilate without dissociation is assumed to be rather large. If this is true, the number of free carriers contributing to PC is effectively reduced. Somewhat different results have been obtained by Gross et al. (1969), who reported an increase of the photoconductivity at an energy $\hbar\omega_{LO}$ higher than that of an exciton. The authors interpreted this observation in terms of hot carriers bound to excitons followed by the thermalization of these excitons due to the emission of LO phonons. Within this approach, it has been suggested that the PC peaks at energies of excitons plus $\hbar\omega_{LO}$ most probably result from excitons bound to defects or impurity centers. Therefore, based on the presented arguments, the origin of the 480-nm band in spectrum 2 of Fig. 15 can viably be connected with bound excitons and in particular with the I_2 exciton.

Fig. 16 summarizes the experimental findings obtained in ZnS samples. The PC spectrum (dashed line) exhibits a weak band between 2.5 and 3.0 eV which may be attributed to sulfur vacancies (Leutwein et al., 1967). Little changes have been observed at subthreshold driving. Increasing the driving amplitude above the threshold value for the SL production results in a pronounced change of the PC spectrum (solid line in Fig. 16) including the appearance of new bands at 3.25 and 3.52 eV and a considerable enhancement of the band near 2.80 eV. These changes completely disappear after removal of the driving.

Additional lines in the spectrum of acoustically driven PC arise from defect complexes of the sulfur vacancy V_S^+ and the interstitial zinc Zn_i^+. Using the Coulomb approximation (cf. Eq. (9)), the energy levels E_n of the complex are given by

$$E_n = E(V_S^+) + e_0^2/4\pi\varepsilon_0\varepsilon r_n\,, \tag{21}$$

where $E(V_S^+) = 2.9$ eV below the bottom of the conduction band is the binding energy of the isolated sulfur vacancy (Georgobiani et al., 1983), and r_n is the separation between V_S^+ and Zn_i^+ for each shell of equidistant defects. The shells are denoted by the integer n. As shown in Fig. 16, the calculated transition energies indicated by arrows are completely consistent with the observed peaks.

Current fluctuations of acoustically driven PC spectra already seen in the spectral range from 2.9 to 3.2 eV in Fig. 16 are much more intense in the acoustically driven PC spectrum shown in Fig. 17. These fluctuations have been ascribed by Ostrovskii and Korotchenkov (1985) to mobile dislocations carrying electric charges. In this context, it is essential to take into account the presence of

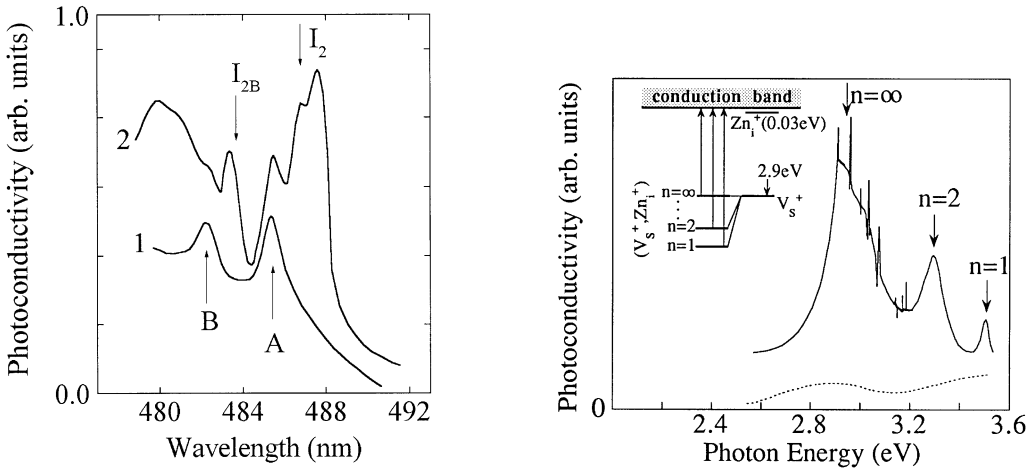

Fig. 15. Photoconductivity spectra of an as-grown CdS platelet at 4.2 K without (1) and with (2) pre-exposition to above-threshold driving. The intrinsic exciton wavelengths are marked by arrows A and B. The I_2 and I_{2B} bound exciton line notation is due to Thomas and Hopfield (1962). The spectra are taken from Ostrovskii and Rozhko (1984).

Fig. 16. Acoustically driven photoconductivity spectra of a ZnS : Ag (10^{-4} at%) sample: dashed line, PC without driving; solid line, PC driven at $U = 1.3U_{th}$. The SL appearance roughly corresponds to an acoustic intensity $w_{th} = 0.5$ W/cm^2. Inset illustrates the energy levels of the (V_S^+, Zn_i^+) defect pair responsible for the observed PC bands. It should be noted that V_S^+ exists as a singly negatively charged sulfur vacancy V_S^{2+} whereas Zn_i^+ is the zinc ion which has captured one electron. The transitions marked by $n = 1$, 2 and ∞ are calculated energies E_n using Eq. (21) at the separations $r_1 = 2.70$ Å, $r_2 = 4.68$ Å and $r_\infty \to \infty$ between defects which have been obtained from the lattice structure parameters. From Ostrovskii and Korotchenkov (1992).

electronic energy levels localized at dislocations and having energies within the band gap in II–VI semiconductor compounds (Petrenko and Whitworth, 1980; Osip'yan et al., 1986). The flow of charge arises from the displacement jumps of charged dislocations across the slip plane and gives rise to fluctuating currents when electrons (holes) are transferred to the conduction (valence) band under illumination. The consistency of the data which are presented in Figs. 16 and 17 and reveal the final spectral ranges of current fluctuations is therefore encouraging in finding the energy levels of mobile dislocations as will be discussed in more detail below.

3.3.3. *Other effects*

In this section, two experimental findings are briefly discussed which give independent information on the approximate energy structure of mobile dislocations in ZnS crystals. The first subject to be discussed will be the experimental work on acoustically driven electron emission from crystal surfaces.

As already mentioned, there exists a number of emission phenomena arising from mechanical effects in solids. The two most intensely studied relevant effects are mechanoluminescence, which gives rise to emission of photons, and acoustic emission which gives rise to emission of phonons.

A great body of empirical evidence is already available showing the emission of particles, in particular electrons, from the surface of mechanically deformed samples (see, for example, Mukhopadhyay, 1984; Zakrevskii and Shuldiner, 1995, and references therein). A complete understanding of the electron emission requires realistic data on such complicated processes as the

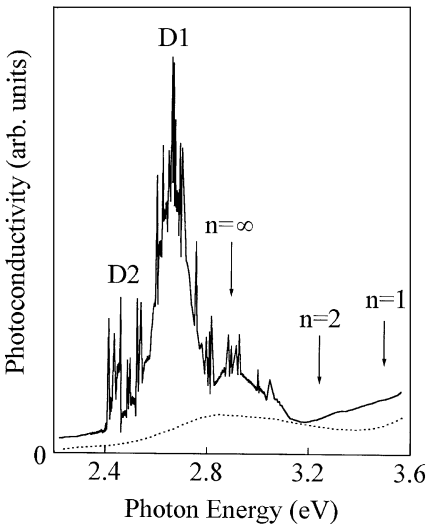

Fig. 17. Acoustically driven photoconductivity spectra of an undoped ZnS sample: dashed line, PC without driving; solid line, PC driven at $U = 1.3U_{th}$. The transition energies denoted by $n = 1$, 2 and ∞ are calculated energies E_n depicted in Fig. 16. The ranges of fluctuating currents marked by D1 and D2 correspond to the dislocation bands exhibited in the inset of Fig. 18. After Ostrovskii and Korotchenkov (1985).

development of cracks and microcracks (Arnott and Ramsey, 1971), the stress-induced diffusion of point defects towards surfaces (Pimbley and Francis, 1961; Claytor and Brotzen, 1965), and the local heating (Rosenblum et al., 1977) which may accompany mechanical effects. Apart from numerous approaches surrounding the interpretation of the electron emission effect, there is one significant issue of particular interest. This concerns the role of dislocations which is of great importance for the interpretation of data obtained in ionic crystals (e.g., Poletaev and Shmurak, 1981; Zakrevskii and Shuldiner, 1995).

The electron emission from a crystal subjected to acoustic driving under a large variety of conditions was first identified by Rozhko (1984) on $LiNbO_3$ plates in vacuum. Later, Ostrovskii and Korotchenkov (1985) obtained data in ZnS samples which were explained by electron emission and which supported the view that charged dislocations moving in acoustic fields are directly involved in the emission process. The authors concluded that electrons gain the energy, required to leave the surface, from the electric field of dislocations. Since illumination of II–VI compounds produces a change in the charge carried by dislocations (Osip'yan et al., 1986), they performed additional experiments in order to test the validity of the model which describes the acoustically driven electron emission phenomenon. To verify the dislocation approach, Ostrovskii and Korotchenkov (1985) measured the spectral distribution of the emitted electron charge.

The crucial experiment is illustrated in Fig. 18. The spectral dependence of the normalized charge density $\Delta Q = Q(\lambda) - Q_{dark}$ shows two minima marked by arrows 1 and 2, and two peaks marked by arrows 3 and 4. Here, Q_{dark} is the emitted charge density in the dark and $Q(\lambda)$ the one due to illumination with light of wavelength λ. The authors argued that the peak positions may closely be linked to dislocation states in the energy gap. Hence, the most likely process appears to be that during the illumination with wavelengths in the range from 400 to 550 nm, the negative

charge on the dislocations decreases due to the excitation of electrons from states at the dislocation core into the conduction band. As a consequence of the decrease of dislocation charges, the amount of the charge emitted from the sample decreases. On the other hand, the infrared light excites electrons from the valence band into the dislocation states and thus increases the negative charge on the dislocations. This is the reason why a pronounced increase in the emitted charge is seen in the spectral range 0.8–1.2 μm in Fig. 18. The fact that two negative and two positive peaks are observed (Fig. 18) suggests that two dislocation levels are likely involved in the emission process.

Using these results, Ostrovskii and Korotchenkov (1985) identified two dislocation bands D1 and D2 which are shown in the inset of Fig. 18. The transitions marked 1 and 2 are those which produce a decrease in the dislocation charge and thus lead to the decreased emitted charge marked by arrows 1 and 2 in Fig. 18 as well as to the current fluctuations in the spectral ranges D1 and D2 of acoustically driven photoconductivity shown in Fig. 17. The transitions marked 3 and 4 in Fig. 18 are then those transitions which increase the dislocation charge and thus lead to the enhanced emitted charge at about 1.33 and 1.05 μm, respectively.

We end this account of acoustically driven defect charges by commenting on the acoustically driven photo-EPR of Cr^+ ions in ZnS crystals. The Cr^+ EPR signal is known to be quenched when the crystals are illuminated with photons of such an energy that the Cr^+ ions are ionized. On the other hand, band-gap illumination is known to enhance the EPR signal due to the capture of electrons from the conduction band into the Cr^{2+} ions (Dieleman et al., 1962; Taki and Bö, 1968).

Gorelov et al. (1985) have shown that the EPR signal of Cr^+ ions is substantially lowered by applying acoustic driving and that the size of the effect can be varied by illuminating the sample. The authors explain their experiments in favor of the dislocation mechanism and claim that the observed ionization of Cr^+ ions and the defect charge redistribution are caused by the electric field of charged dislocations. To enlighten this subject further, it might therefore be useful to compare acoustically driven photo-EPR data with the spectral change of emitted charge which has been discussed previously.

A comparison of such spectra is shown in Fig. 19. For the benefit of the reader, a part of the spectrum of the acoustically driven emitted charge presented in Fig. 18 is redrawn in Fig. 19 (closed circles). The open circles in Fig. 19 represent the spectral distribution of the relative change of the EPR signal, $(I^+_{Cr}(U) - I^+_{Cr}(0))/I^+_{Cr}(0)$, where $I^+_{Cr}(U)$ and $I^+_{Cr}(0)$ are the EPR signal intensities at the driving amplitude U and $U = 0$, respectively. A clear correlation of the spectral behavior of the emitted charge and acoustically driven photo-EPR is readily seen. This proves that driving affects the photo-EPR data in a manner which is predicted by the concept that the variation of the dislocation charges due to the illumination of the sample changes the electric field strength associated with dislocations and, hence, alters the Cr^+ ion ionization probability.

It is therefore fair to say that the bulk of direct and indirect evidence seems to support the model of acoustically driven defect charges. The model of acoustic driving as discussed in this article can, however, also be applied in other contexts. Interested readers may examine, for example, the work on the dramatic increase of PL intensities in polycrystalline silicon initiated by ultrasound and interpreted in terms of defect dissociations and diffusion mechanisms (Koshka et al., 1996). Other examples are acoustically driven optical effects in HgI_2 due to dislocation pinning centers (Kardashev, 1996), the change of the photosensitivity in CdS crystals originating from acoustically stimulated motions of shallow donors (Sheinkman et al., 1995), the acoustically stimulated dissociation of iron–boron pairs in silicon (Ostapenko and Bell, 1995), the ultrasound regeneration of EL

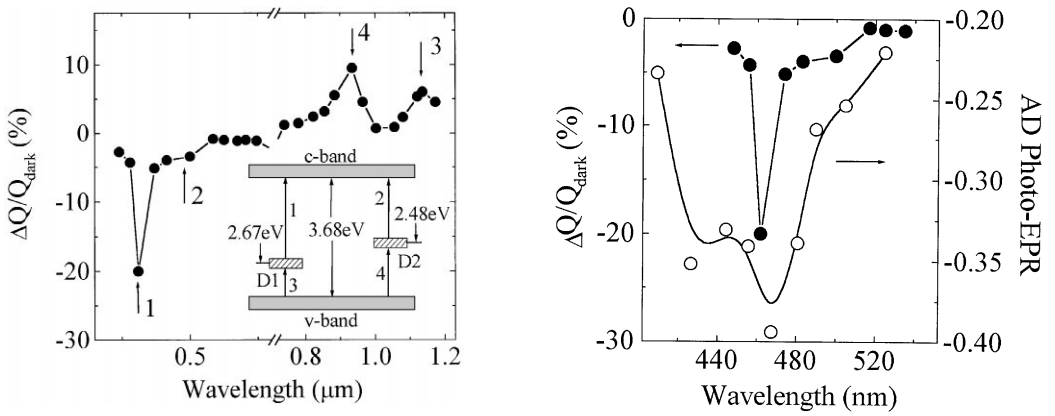

Fig. 18. Typical changes of the electron charge emitted from the surface of a ZnS : Ag (10^{-4} at%) sample in vacuum due to the illumination with different wavelengths. The dark charge is $Q_{dark} \approx -2.7 \times 10^{-10}$ Q/cm^2. The inset shows approximate positions of the energy bands D1 and D2 of mobile dislocations in a ZnS sample as estimated from acoustically driven electron emission and photoconductivity data. Arrows 1–4 in the figure exhibit calculated wavelengths of the electronic transitions 1–4 presented in the inset. After Ostrovskii and Korotchenkov (1985).

Fig. 19. Spectral dependence of the acoustically driven electron emission (closed circles, from Fig. 18) and the quenching of the Cr^+ EPR signal (open circles) in a ZnS : Ag (10^{-4} at%) sample. The open circle data are taken from Gorelov et al. (1989).

centers in GaAs (Buyanova et al., 1994a), the ultrasound effect on the dislocation-related photoluminescence in Si/Ge_xSi_{1-x} heterostructures due to ultrasound-stimulated dislocation gettering and reorientation of the impurities (Buyanova et al., 1994b), as well as the novel approach of influencing spectroscopic properties of semiconductor clusters by ultrasound (Spanhel and Anderson, 1991).

Acoustic driving is a unique technique for generating associated pairs of lattice defects in crystals and of producing internal electric fields of considerable strengths. By observing SL and acoustically driven optical effects, it is clear that moving dislocations are the principal agents of optical phenomena in solids subjected to driving. The underlying complex physical process of defect production due to driven dislocations still lacks from a complete atomistic description. In many ways, a better understanding of these properties could have important implications on the large-scale mechanical behavior of solids. Open questions of both fundamental and technological relevance like plasticity, fracture, the brittle versus ductile behavior of materials are typical examples in this context.

4. Sonoluminescence at solid–gas interfaces

Another convincing test for the validity of the model of acoustically driven defect charges stems from the observation of sonoluminescence at solid–gas interfaces. The key issue here is how the sonoluminescence is affected by further increasing the driving amplitude. Ostrovskii and Rozhko (1985) have shown that a sharp-line SL spectrum is observed when the rf driving voltage U in a CdS

plate is further increased. The emission extends from 400 to 710 nm and is suggested to originate from atoms and molecules adsorbed at the crystal surface. A closer inspection of the SL spectrum presented in Fig. 20 reveals that it may originate from hydrogen. This interpretation is most evident for the part of the spectrum which is shown by the dashed curve. The emission is very similar to the Q branch of hydrogen-containing molecules with peak energies (Herzberg, 1945)

$$E = E_0 + 2\pi(B' - B)\, j + 2\pi(B' - B)\, j^2 \,. \tag{22}$$

Here, $B' = 17.3\,\mathrm{cm}^{-1}$ and $B = 14.18\,\mathrm{cm}^{-1}$ are the rotational constants of the molecule. E_0 is a constant and $j = +1, 2, 3, \ldots$

The SL spectrum exhibited by the dotted curve in Fig. 20 is dominated by the singly ionized N_2^+ nitrogen molecule. The peak energies are well described by

$$E = E_0' + 2\pi(B' + B)\, j + 2\pi(B' - B)\, j^2 \,, \tag{23}$$

where $B' = 2.108\,\mathrm{cm}^{-1}$ and $B = 1.962\,\mathrm{cm}^{-1}$ correspond to the rotational constants of the N_2^+ molecule (Herzberg, 1945). We also like to mention that the appearance of helium-related lines in the SL spectrum of the CdS/He interface has previously been observed by Ostrovskii and Rozhko (1985; see also Rozhko and Gnatenko, 1991).

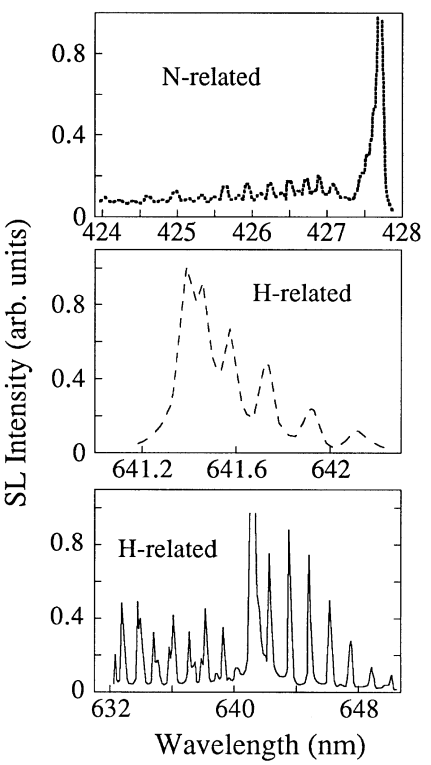

Fig. 20. Part of the SL spectrum obtained from a CdS platelet in a liquid helium continuous-flow cryostat exhibiting emission lines from a hydrogen-containing molecule and the singly ionized N_2^+ nitrogen molecule (after Ostrovskii and Rozhko, 1985).

The most rigorous approach to understand the physical processes involved in the observed emissions has been performed by Ostrovskii and Das (1997) by analyzing the data obtained at $LiNbO_3$/air and CdS/He interfaces. In what follows, the $LiNbO_3$/air interface will be used as an example. This interface has been found to emit sharp SL lines in the violet and near ultraviolet as shown in Fig. 21. The appearance of the N_2 molecule lines is the most striking feature of the spectrum. One might be tempted to identify the observed emission as an air discharge in piezoelectric fields arising from the driving. However, this interpretation is still open for discussion.

At this point, two comments are in order. First, the piezoelectric field strength near the surface of the plate maintaining resonant vibrations is given by Eq. (7). In this way, the threshold field for initiating an air discharge at atmospheric pressure has been determined to be 5.85×10^3 V/cm (Ostrovskii and Das, 1997). This value appears to be remarkably low considering that threshold electric fields as high as 10^5 V/cm have been reported for the air discharge at atmospheric pressure when excited by short electric pulses (Stearns, 1990). Owing to the lack of detailed data on air discharges in rf electric fields, we can only note that such a discharge has been observed at much lower pressures of 0.2–20 Torr in fields of 1.5×10^3 V/cm (Hatch and Heuckroth, 1970). It is therefore believed that it is rather improbable to attain self-sustained air discharge at the estimated piezoelectric field strengths.

Second, SL at a solid–gas interface appears as luminous microspots with typical dimensions of a few μm which move across the sample surface when tuning the driving frequency. Another prominent feature of SL is that it arises at flat polished surfaces without metal electrodes for initiating the discharge near the surface. We therefore believe that the estimated piezoelectric field F_{piezo} is realistic and that the field strength at the surface of the driving plate is not locally increased.

An interesting explanation of the observed SL has been offered by Ostrovskii and Das (1997). They assume that the SL occurs as a gas discharge phenomenon in the vicinity of the solid–gas interface due to high electric fields provided by acoustically driven charged dislocations. As already pointed out, the existence of dynamic charges at dislocations has been proven experimentally and electric field strengths of the order of 10^5 V/cm have been reported to exist near dislocation cores (Osip'yan and Petrenko, 1986). Future studies of the SL phenomenon at solid–gas interfaces should therefore use a model that accounts for the dynamic dislocation charges. It is, however, fair to say that until now "surface effects" of this type have barely been studied. A better understanding of the consequences of this exciting phenomenon is still needed.

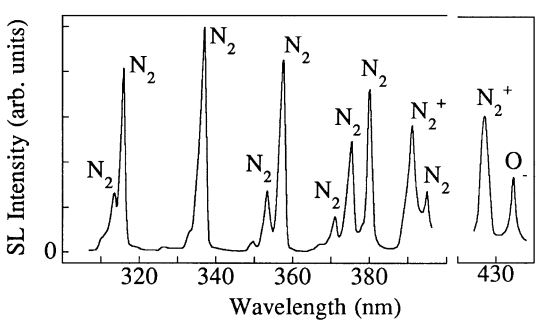

Fig. 21. Spectrum of SL from a $LiNbO_3$ / air interface at 300 K with line assignment (after Ostrovskii and Das, 1997).

In this section, we have outlined the SL which arises from a gas discharge at solid–gas interfaces. The phenomenon as such seems to be applicable in a variety of disciplines. Since the effect, in principle, is rather simple it could be used as an initializer of microdischarges in gases. In particular, its use in fluorescent lamps and displays is rather obvious. More generally, there is a considerable potential for exploiting clean plasma chemistry technologies which could be made more efficient with acoustically initiated gas discharges. Another example is the development of a cheap sensor for the detection of gases. It is this kind of devices that may lead to future commercial applications in environmental pollution monitoring.

5. Sonoluminescence in granular materials

5.1. Why are sonoluminescence effects in granular media interesting?

As mentioned earlier, the key processes in describing SL phenomena are governed by complicated dynamical properties of air bubbles in water or dislocations in solids. It has long been recognized that mixtures of granular media give rise to a variety of remarkable phenomena which exhibit both fluid and solid aspects and are driven by amazing dynamical properties (for a review, see Jaeger et al., 1996). Among the subjects of increased recent interest for physicists is the mixture response to externally applied vibrational excitations. This response is an important fundamental property of granular media which is relevant to the classical scope of physics as well as to many other technologies, such as mechanical processing in pharmacology, engineering, etc.

It is worth emphasizing here that effects observed under vibrations are of particular importance for the understanding of granular flow phenomena since both vibrations and flow are largely governed by intergrain collisions. Such collisions are dissipative implying that applications of molecular dynamics analysis are restricted to grain systems. Due to the seductive complexities of granular materials, an acceptable general theory for granular flows has not yet been developed. The greatest theoretical effort has been devoted to the comparison of granular flows with simple molecular systems (e.g., Haff, 1983; Lun et al., 1984). It should, however, be noted that in a standard vibration experiment with frequencies on the 1 Hz scale, the energy is supplied to a granular system which is contained into a bed with perpendicular motion of a wall. This implies that the motion is large compared with the grain diameter and that coherent grain motions most likely occur near the wall. The experimental verification of granular hydrodynamics is therefore rather complicated since it is difficult to obtain a precise analogy to the molecular energy transfer with random vibrations of molecules at the surface of the wall.

For this reason, a new approach for studying granular dynamics has recently been proposed (Korotchenkov and Goto, 1997). It is anticipated that a random velocity field is produced when exposing a mixture of grain particles to a MHz frequency oscillating plate. Uncorrelated eddying particle motions are likely maintained near the plate boundary layer thus leading to a fluidization of the upper layers of a granular mixture and giving rise to enhanced mechanical interactions between grain particles. The latter fact has been shown to be capable of producing grain collision-induced light emission, i.e. sonoluminescence in a granular mixture of ZnS or ZnS : Mn particles originating from a near surface region of the grains. This observation raises new and

fascinating issues for studies of granular media since it may provide interesting information on such important quantities as the collision rate, slipping friction of granular particles, pressure at the surface of the grains, etc. SL studies do not only provide the direct imaging of particle dynamics, but have also significant implications on the exploration of granular friction which is a topic of increasing interest since it is of great importance for the understanding of earthquake dynamics (Carlson et al., 1994; Nasuno et al., 1997).

5.2. Observing sonoluminescence in granular mixtures

Fig. 22 shows a typical experimental setup. A granular mixture is tightly packed into a cylindrical glass-walled flask, typically 6 mm in diameter and about 1 mm in depth, and closed with two plates. The lower plate is made of glass while the upper one is a Y- or 41° Y-cut $LiNbO_3$ piezoelectric plate which provides the oscillating driving. The lower surface of the $LiNbO_3$ plate is covered with a thin semitransparent metal electrode in order to screen piezoelectric fields. A further electrode is fixed to the upper surface of the plate. Maximum spectral range is obtained by removing the lower electrode and by depositing a pair of stripe electrodes onto the upper and lower surface of the plate. After applying an rf voltage U to the electrodes, Z-propagating plate acoustic waves are generated in the $LiNbO_3$ with a mixture of vertical and horizontal displacements at the plate surface (Viktorov, 1967; Solie and Auld, 1973). In these experiments, the lowest plate modes from 1 to 6 MHz have been employed.

The cell is vertically oriented and closed with a screen. The screen is separated by a gap of approximately 0.5 mm from the $LiNbO_3$ plate and tilted in the base plane in such a way that the sound in the plate propagates along the axis which is typically $\Phi = 20$–$40°$ off the vertical direction, as shown in Fig. 22b. Sonoluminescence is observed at sufficiently high driving amplitudes. The emission is transmitted by a transparent $LiNbO_3$ plate and imaged onto two-dimensional 576×384 CCD cameras (Princeton Instruments).

Sonoluminescence (a) and photoluminescence (b) spectra of ZnS : Mn and ZnS grain mixtures are compared in Fig. 23. The dramatic difference between the SL and PL emission is clearly seen. Of particular interest is the prominent PL band of the Mn^{2+} ion yellow emission (Langer and Ibuki, 1965) at about 585 nm in the ZnS : Mn samples (Fig. 23b) and the blue self-activated

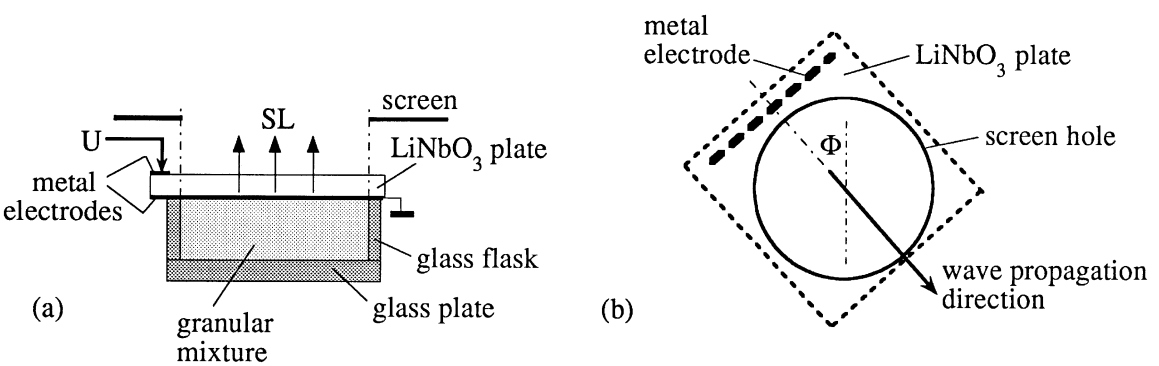

Fig. 22. Schematic of the side (a) and top (b) views of the setup for observation of SL in granular mixtures.

emission at about 450 nm (Samelson and Lempicki, 1962) in pure ZnS (Fig. 23b) which are not observed in the SL spectra (Fig. 23a). Considering these facts, it is interesting to note that highly doped ZnS : Mn crystals exhibit an emission band at about 800 nm (Tong and Goede, 1983; Benoit et al., 1984). This band has tentatively been ascribed to optical transitions involving intrinsic defects although the nature of the defects is not definitely known. Fig. 23b shows a similar band on the long-wavelength side of the Mn^{2+} emission tail of the PL spectrum of ZnS : Mn. Furthermore, the SL spectrum of ZnS : Mn in Fig. 23a displays a pronounced emission peak close to 800 nm. A closer examination of the SL spectrum of ZnS in Fig. 23a reveals a weak band in the range between 600 nm and about 850 nm. This implies that the PL spectrum of undoped grains in Fig. 23b may show some evidence for a subsidiary emission above 570 nm suggesting the participation of defects in the SL of undoped grains. Based on the presented evidence and taking into account the fact that the Mn^{2+} d-electron states are known to act as effective luminescence centers, it is rather unlikely that the SL originates in the interior of the grains. The region near the surface has therefore been suggested by Korotchenkov and Goto (1997) as the origin of the observed SL as pointed out earlier.

It should be noted that the near plate disturbances at acoustic driving are damped in the interior of the mixture by grain collisions which are inevitably inelastic and not central, so that frictional forces are exerted. Hence, increased pressure, induced electric fields and localized heating of rubbing particle surfaces are possible candidates for the explanation of the light observed in sonoluminescence. There are therefore reasons to describe SL in terms of granular dynamics.

5.3. Granular dynamics and sonoluminescence effects

One of the key issues is the relevance of the sonoluminescence emission with respect to the underlying complex movements of grains inside the container due to acoustic driving. Without a detailed analysis, we intent to discuss this problem by comparing the dependence of the total SL intensity and the corresponding evolution of the SL images upon the increasing driving amplitude as illustrated in Figs. 24 and 25, respectively. The SL images displayed in Fig. 25 are remarkable in the sense that the distribution of the emission intensity is highly heterogeneous. At sufficiently low driving amplitudes (well below $U = 50$ V in Fig. 24), SL appears to originate from regions with typical dimensions of a few hundreds μm (green and yellow dots in Fig. 25a and Fig. 25b) close to

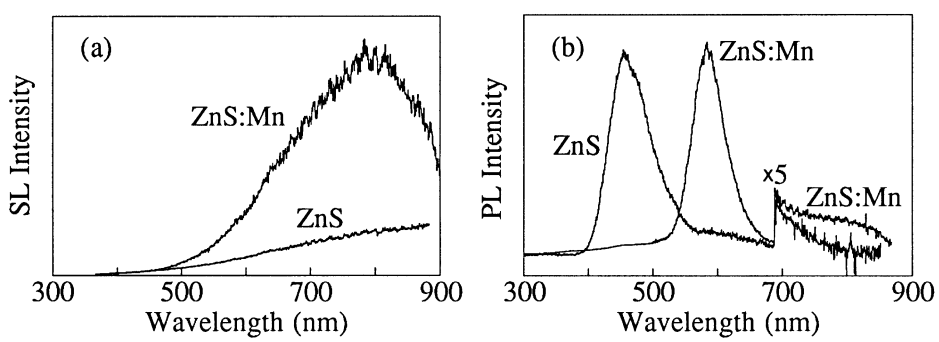

Fig. 23. Comparison of the spectra of SL (a) and PL (b) from ZnS : Mn and ZnS granular mixtures taken at room temperature, $U = 68$ V and $f \sim 3.4$ MHz (after Korotchenkov and Goto, 1997).

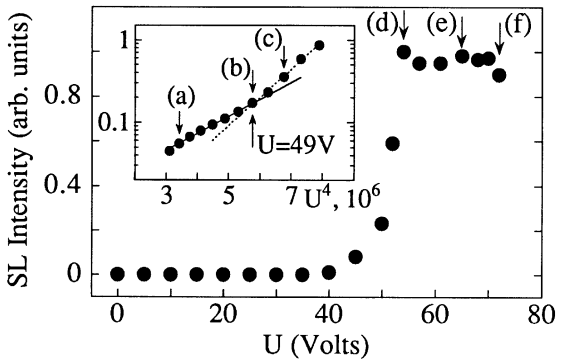

Fig. 24. Dependence of the total image computed SL intensity on the driving voltage U for a ZnS : Mn grain mixture at frequency f of about 3.4 MHz. The grains are of slightly anisotropic shapes with linear dimensions differing not more than a factor of 1.5–1.6 and centered at about 3 μm. The inset shows the logarithm of the SL intensity as a function of U^4 for the data presented in the figure. The solid and dashed lines in the inset are the exponential fits to the data points which they intersect. From Korotchenkov and Goto (1997).

the edge of the driving electrode. It has been argued that these observations reflect the tangential particle flow along the interface boundary caused by the acoustic field and resemble the tangential boundary viscosity stream effect that is produced by a harmonically varying movement of a sound source (Nyborg, 1965; Moroney et al., 1991). Another issue that needs to be addressed here is the gravity force which is known to play an important role in granular dynamics (see Jaeger et al., 1996 and references therein). The gravity force should influence the viscosity movement of grains across the wave axis resulting in an expansion of the image along the vertical axis, as is the case (Fig. 25).

As the driving amplitude increases above $U = 50$ V, the SL intensity grows and generates black regions of considerable enhanced intensity (Fig. 25c–Fig. 25f). The probably most realistic explanation for the occurrence of these regions is the formation of grain aggregates which are organized by particles slipping into available voids. In the model discussed here, this should increase the SL intensity due to an increased collision rate of grains within the aggregates. It might be expected that the change in the total SL intensity would occur at roughly the same driving amplitude. This expectation is reasonably well met in Fig. 24 exhibiting a very rapid increase of the SL intensity above $U = 50$ V.

It should be noted that the results presented here are qualitatively in agreement with grain dynamics. For a quantitative approach, let u be the average velocity of a grain near the driving wall, ξ the average spacing between nearest grains, and m and σ the mass and radius of the grains which are assumed to be identical. Using the molecular kinetic approach (Haff, 1983), the pressure exerted by the driving plate is given by

$$P \propto mu/t_0(2\sigma)^2 , \tag{24}$$

where $t_0 \propto \xi/u$ is the average time between grain collisions. Here, the average grain velocity near the driving surface has been approximated by assuming

$$u \propto fa_0 \propto U , \tag{25}$$

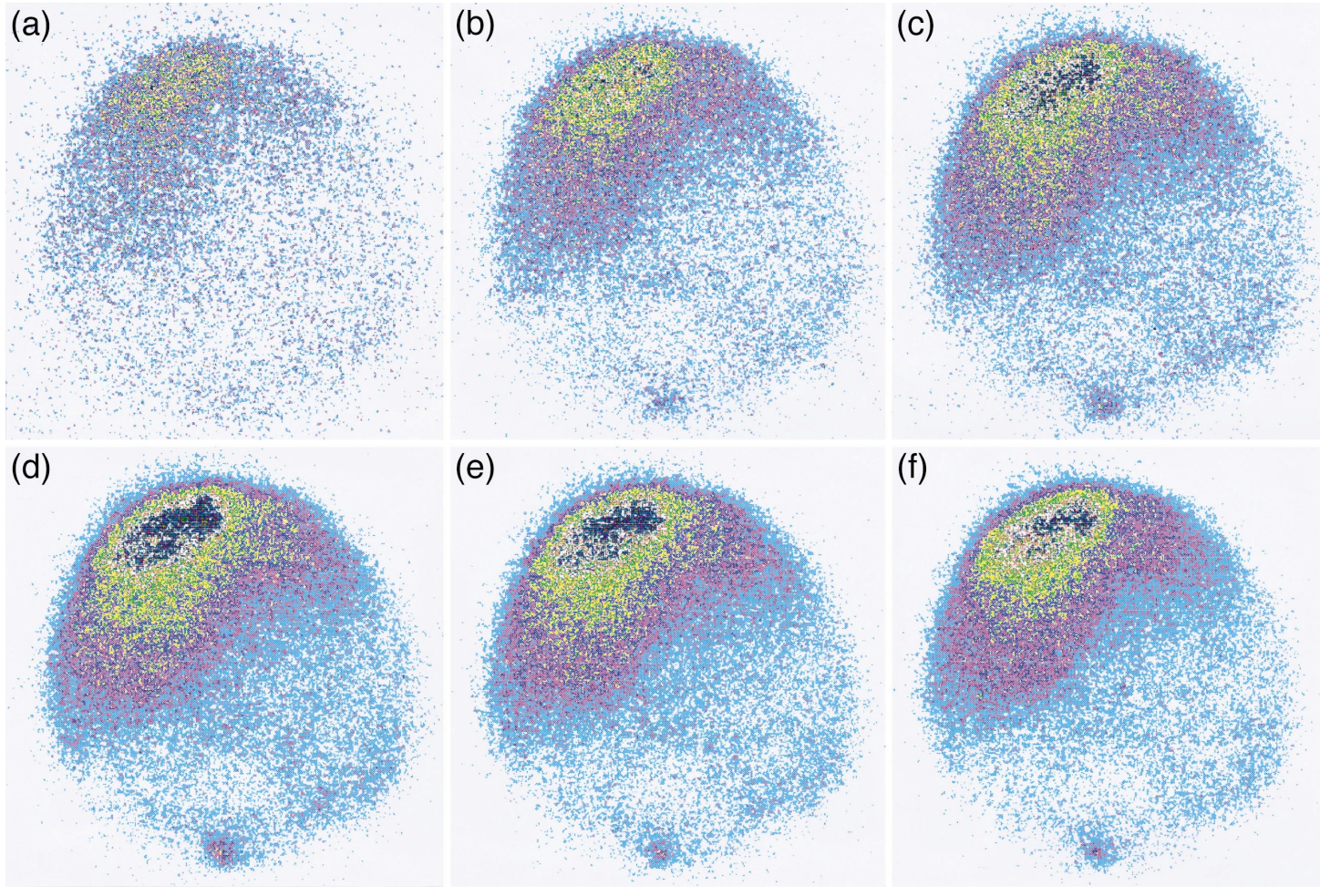

Fig. 25. Evolution of the CCD images of ZnS : Mn SL with gradually increasing driving amplitude from a to f. The driving voltage U is denoted by arrows a–f in Fig. 24. The color scheme is black → yellow → magenta → green → blue → white for maximum to minimum SL intensity. The cell orientation relative to the vertical axis and acoustic wave propagation direction corresponds to that depicted in Fig. 22b. The 6 mm diameter image spans about 340 pixels.

where a_0 is the amplitude of the surface motion and f is the frequency of the ultrasonic wave. The pressure P may then be taken as

$$P \propto 2\sigma\rho U^2/\xi\,, \tag{26}$$

where $\rho \propto m/(2\sigma)^3$ is the density of the grain mixture. Eq. (26) shows that enhanced pressure is exerted in the grain system by increasing the driving voltage U and decreasing the average spacing ξ between nearest grains.

An estimate of the SL intensity I_{SL} is derived from studies of the pressure-induced luminescence of ZnS : Mn phosphors (Alzetta et al., 1962) and can be expressed as $\ln I_{SL} \propto P^2$. This finally leads us to

$$\ln I_{SL} \propto (2\sigma)^2\rho^2 U^4/\xi^2\,. \tag{27}$$

If the data, which have been taken in the region exhibiting the pronounced increase in the SL intensity, are plotted as $\ln I_{SL}$ vs. U^4, they reduce within the experimental error into two linear curves as expected (see inset of Fig. 24).

It is therefore concluded that Eq. (27) is reasonably accurate for further discussions. As expected, the pronounced change in the intensity dependence shown in the inset of Fig. 24 occurs roughly at $U = 50$ V. The increase of the slope above the break point (marked by the arrow) reflects the decrease in the average spacing ξ between nearest grains in accordance with Eq. (27). This in turn may suggest that the SL intensity increase at about 50 V in Fig. 24 originates from regions of closely packed grains and that this fact is consistent with the observation of a heterogeneous image (Fig. 25c–Fig. 25f). Within the aggregates, the collision rate which is proportional to ξ^{-1}, is expected to enhance but the grain velocities u should decrease. The rate of energy loss through grain collisions (Haff, 1983),

$$\mathrm{d}W/\mathrm{d}t \propto \rho u^3/\xi\,, \tag{28}$$

is therefore assumed to decrease eventually quite considerably. It is thus expected that the SL should rise quite abruptly and then exhibit a very slow increase or even saturate at some level of intensity. Fig. 24 clearly indicates that this is indeed observed. By analyzing the images d, e and f of Fig. 25, a gradual decrease of the light emission is noticed from the black regions of enhanced SL which is fully consistent with the SL intensity saturation observed between arrows d and f in Fig. 24. Evidently, such a behavior is in excellent agreement with the presented model of intergrain interactions.

The variation of packing density of grains with U can be treated numerically using the data of Fig. 24. For spherical particles, the packing fraction $\eta = (4/3)\pi\sigma^3/$ (volume per grain in a mixture) has been found to vary from $\eta \sim 0.56$ for the random loose packing to $\eta \sim 0.64$ for the tightest, random close packing of particles (Onoda and Liniger, 1990). If the volume per grain in a mixture is approximated by $(4/3)\pi(\sigma + \xi/2)^3$ and the lowest packing fraction $\eta_0 \sim 0.56$ is attributed to the slope of the solid line in the inset of Fig. 24, the solid and dashed line fits yield the intergrain separations $\xi_0 \sim 0.64$ μm and $\xi_1 \sim 0.49$ μm, respectively. This gives a packing fraction of $\eta_1 \sim 0.63$ for the slope of the dashed line which is consistent with the upper limit of the random close packing reported by Onoda and Liniger (1990). These results strongly support the model which ascribes SL excitation to grain dynamics.

In summary, the data discussed so far serve as a good starting point for the exploitation of the SL phenomenon in granular medium, though this research field is still in its infancy. In fact, the presented results raise as many questions as they answer. In particular, the question, how much

insight one may obtain from the dynamics of the inner layers of a granular system subjected to the driving plate, remains still unanswered and demonstrates the limitation of the developed techniques. However, regardless of what the ultimate implementation of the presented observations turn out to be, one thing seems to be clear: Sonoluminescence studies provide convenient means for a better understanding of granular dynamics. Among the intriguing possibilities, it is expected that useful insights into particle slipping events and associated fluidization of granular systems may emerge from these studies.

6. Acoustically driven radiative recombination dynamics in bulk semiconductors and low-dimensional structures of semiconductors

6.1. Acoustic charge transport and storage of light in quantum wells

Although much is known experimentally and theoretically about the dynamics of photogenerated carriers in semiconductors, relatively little attention has been given the effects of acoustic driving on the dynamics of carriers. Based on photoluminescence studies in InGaAs/GaAs quantum wells, Rocke et al. (1997) have shown that extremely long lifetimes of optically excited carriers are achieved with acoustic drivings. In this chapter, we intent to give a better understanding and interpretation of the basic ideas behind acoustically driven carrier lifetimes. Though this will be relatively simple, these ideas are nevertheless of great conceptual importance, because lifetime parameters can be considerably influenced by the driving without affecting the superior optical quality of materials.

In the studies reported by Rocke et al. (1997), the excitons confined in an InGaAs quantum well have been affected by a moving piezoelectric potential of a surface acoustic wave (SAW) generated in the GaAs substrate of the sample structure and propagating along the plane of the quantum well. Within the piezoelectric field of the wave which can be as high as 10 kV/cm, the excitons polarize and finally dissociate into electron–hole pairs at sufficiently high fields. The dissociated pairs are transferred to the potential wells associated with the traveling wave. These stored charges are then transported over macroscopic distances at the velocity of a SAW. With transport channels of the order of 1 mm which is typical for modern multilayer structures, and the SAW velocity of about 3×10^3 m/s, an acoustic delay time of the order of 0.5 μs is expected. Screening the wave potential well by covering the exit of the transport channel with a metal layer, restores the electron–hole pairs into excitons which triggers the radiative recombination and allows μs-prolonged recombination times.

The basic physics is summarized in Fig. 26 which also illustrates the idea of Rocke et al. (1997). The SAW pulse of 200 ns width is generated at the time $t = 0$ by using an interdigital transducer IDT (for details on IDTs see, for example, Joshi and White (1969) and, Ponamgi and Tuan (1975)) and travels to the right as sketched in the inset of Fig. 26. At about $t = t_1$, the SAW pulse is centered at the point $x = x_{in}$ where a laser pulse produces electron–hole pairs. The electric field of the SAW confines the charges into the wave packet which transports the electron-hole pairs into the active channel of the sample. The transport channel is $x_{out} - x_{in} = 1$ mm long which corresponds to an acoustic delay time $t_{storage} = 350$ ns if the SAW velocity is taken as 2.865×10^3 m/s for

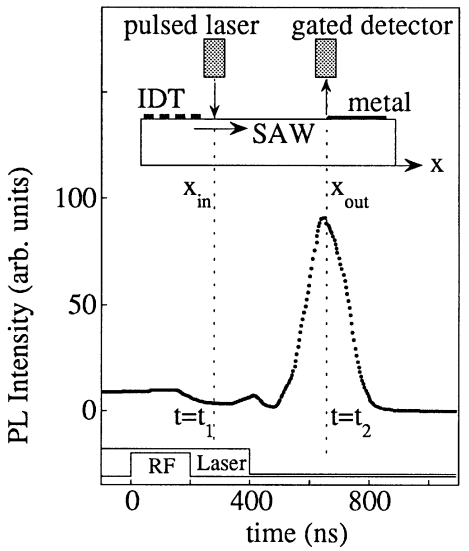

Fig. 26. PL intensity of a single 10 nm wide $In_{0.15}Ga_{0.85}As/GaAs$ quantum well structure as a function of time after SAW excitation. The inset illustrates the experimental setup. The quantum well is grown on a 1 μm thick GaAs buffer (upper face in the inset) and covered by a 20 nm thick GaAs cap layer. This active area of the sample is formed on a (1 0 0)-GaAs substrate and etched into a mesa with an interdigital transducer IDT at its end. At $t = 0$ a 200 ns long rf pulse at $f_{SAW} = 840$ MHz applied to IDT generates a SAW packet with an acoustic power of 13.5 dB m. At $t = t_1$ and $x = x_{in}$, the potential extrema of the SAW are filled with photogenerated electron-hole pairs which are transported with sound velocity to a semitransparent metallization at $x = x_{out}$. Here, the deliberate screening of the piezoelectric potential modulation lifts the spatial separation of the carriers and induces radiative recombination at $x = x_{out}$ and $t = t_2$. The duration of the rf pulse and the laser pulse are indicated in the lower part. Reproduced with permission from Rocke et al. (1997). (The inset of the original figure has been modified)

the given sample cut and orientation. After the delay time, the SAW pulse reaches the point $x = x_{out}$ where SAW fields are screened by a metal layer inducing radiative recombination of the electron–hole pairs which are released from the SAW packet. As seen in Fig. 26, a strong PL signal is observed about 650 ns after the SAW pulse is launched which roughly corresponds to a 350 ns delay between the laser pulse excitation and the light emission. By moving the metal layer across the transport channel, the light storage time can be varied. It is essential to note that about 70% of the carriers photogenerated at $x = x_{in}$ participate in the light emission at $x = x_{out}$ which suggests a remarkable efficiency of the light storage.

Historically, the SAW unipolar charge transport concept (Hoskins et al., 1982) has proven to be particularly useful for high-speed signal processing (Tanski et al., 1988). Today, the demonstration of the ambipolar charge transport with a subsequent recombination at dramatically prolonged times offers a new way of tailoring multilayer structures.

6.2. Acoustically driven internal electric fields imposing on bound exciton lifetimes

We finish this report on acoustically driven recombination dynamics by commenting on the lifetimes of bound excitons in CdS crystals. This two-particle system of a negative and a positive

charge bound to a local potential has been an extraordinary fascinating subject for decades. An exciton bound to a quantum dot is the experimentally as well theoretically most important realization of such a system at present. Many studies use bound excitons for determining the purity of crystals and impurity contents (Dean, 1982; Lu et al., 1990; Reynolds et al., 1995). The recently discovered optical gain and laser emission in II–VI semiconductor structures generated by localized excitons (Ding et al., 1992) has greatly increased the interest in manipulating oscillator strength or lifetimes of exciton systems. These parameters are known to be of particular relevance for optoelectronic devices since, for example, the gain of lasing transitions is inversely proportional to the spectral half-width. It is therefore expected that the number of studies on how the dynamics of radiative recombination of excitons can be externally influenced will grow.

It has been shown previously that externally applied electric fields may quite considerably affect the lifetime of the bound exciton system (see, for example, Bastard et al., 1983; Polland et al., 1985; Zrenner et al., 1994; Wen et al., 1995). Anticipating the acoustic driving generates the internal electric field, the question arises how large the effect of the driving on exciton lifetimes has to be. An attempt to answer this question is illustrated in Fig. 27a which exhibits the decay time of the photoluminescence line of the I_1 exciton bound to a neutral acceptor (Thomas and Hopfield, 1962) as a function of the acoustic driving amplitude. The PL decay time initially increases with increasing U below the value marked by the arrow a in Fig. 27a. Above this value, a pronounced decrease in the decay time appears. The measured decay time of low-temperature PL is generally assumed to be the true lifetime of the bound exciton. Therefore, the data presented in Fig. 27a indicate acoustically driven changes of the I_1 exciton lifetime. In spite of the changes of the lifetime, the luminescence intensity does not change much as shown in Fig. 27b which suggests that the influence of nonradiative processes on the exciton lifetime is small. It is further assumed that a possible influence of thermal effects due to the driving is negligible since the lifetime of bound excitons, contrary to the one of free excitons, is expected to be independent of temperature below ~ 20 K. With increasing temperature, a decrease of the luminescence intensity is anticipated due to the ionization of the bound excitons. This is, however, not observed as demonstrated by the data presented in Fig. 27.

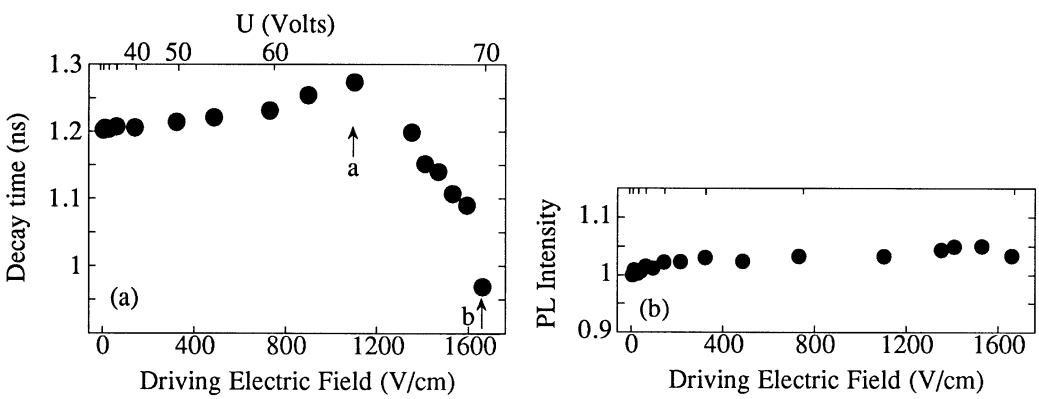

Fig. 27. Lifetime dependence of the I_1 emission line in CdS platelets on varying amplitude of acoustic driving (a) and simultaneous changes of the integrated emission intensity in the I_1 lines, (b) at 4.2 K. The scale of the electric field has been defined by fitting the accompanying absorption edge shift to Eq. (20). After Korotchenkov and Goto (1998a).

Let us now return to our original problem, the electric field of acoustically driven defect charges. We are tempted to describe the lifetime changes as an electric-field effect, since the lifetime τ of excitons trapped by a local potential is given by (Rashba and Gurgenishvili, 1962; Henry and Nassau, 1970)

$$\tau = C/\omega\lambda^3 \, |\psi_0|^2 \, . \tag{29}$$

Here, C is a constant of proportionality, ω is the transition energy, λ denotes the range of the local potential which binds the exciton, and $|\psi_0|^2$ is a measure for the probability of finding an electron and hole on the same site, i.e., the electron–hole wave function overlap. The variation of $|\psi_0|^2$ with the applied electric field as elaborated by Blossey (1970, 1971) provides an approximation which is also applicable to our case. By using his results in the electric field range applied in our studies (cf. the field scale in Fig. 27), one finds that the lifetime should increase to about 1.22 ns at $U = 60$ V. However, Fig. 27 shows that the experimentally observed enhancement of τ is considerably higher.

This raises the question: why is the effect of the driving so much larger? Two approaches are conceivable: (1) there is, of course, the possibility that the electric field strengths attained in our studies have been underestimated. In this respect it should be noted that the field scale of Fig. 27 is defined by a plausible, but approximate, description of the absorption edge shift similar to the one exhibited in Fig. 14. The method sacrifices much of the detailed information on exciton effects in absorption edges. However, the method is designed to focus on the highest long-range electric fields exerted by the driving, as described in Section 3.3. At this point, a simple dimensional estimate is in order. It has been shown experimentally that impact ionization of excitons in II–VI compounds causes the electric-field quenching of exciton luminescence (Harada and Morigaki, 1972; Razbirin et al., 1973). If the energy $m^*\mu^2F^2/2$ gained by the free electrons of mobility $\mu \sim 3 \times 10^4$ cm^2 V/s (Rode, 1970) from the field F is attributed to the dissociation energy of the I_1 exciton which is about 50 meV, the resulting ionization threshold is about 1.1 kV/cm. Assuming the field scale is well defined, the experimentally observed threshold field is close to 1.7 kV/cm, i.e. somewhat larger than the calculated one. However, considering the uncertainty of the assumptions made, the agreement may yet be considered as fairly good. It is therefore rather unlikely that the actual field strength is underestimated by the field scale of Fig. 27.

The second approach to explaining the results in Fig. 27 is based on the assumption that the local field strength at the luminescent center considerably exceeds the field strength presented in Fig. 27. We therefore distinguish between the long-range electric fields and the short-range nonuniform microfields generated by the driving. When it comes to investigating the absorption edge shift, the fitting to Eq. (20) bears significance to the long-range fields. However, the microfields are most probably also involved in the observed lifetime changes. Exactly what sources of the microfields are at issue is a bit subtle. However, there exists a convincing body of empirical evidence in support of the latter possibility. This is true for short-range electric fields of acoustically driven charged dislocations, as discussed previously, and the ones of lattice defects which experience relative displacements in surroundings vibrating at the frequency of external drivings (Korotchenkov and Grimmeiss, 1995). We further assume that microfields occurring at short-range distances cannot be treated in the uniform-field approximation thus precluding the possibility of a direct ionization of excitons which needs sufficiently high electric fields of the order of 140 kV/cm (Blossey, 1970).

With respect to the microfield disturbances imposed by oscillating lattice defects, a few reports are worth to be mentioned briefly. Among those are the findings of Korotchenkov and Grimmeiss (1995), who reported on acoustically driven electron emissions from Se and Te donors in silicon which they studied by using the DLTS technique. The basic result of this study is exhibited in Fig. 28 which shows the enhanced thermal emission rates of these impurity centers in acoustic fields.

In order to understand the observed enhancement, it is useful to discuss the thermal excitation of electrons from deep donor centers in adiabatic approximation. Fig. 29 shows the energy configuration diagram of such a center. The upper and lower solid curves represent the ionized center and its bound state, respectively. For deep impurity centers with pronounced lattice relaxations, the multiphonon excitation process is followed either by a tunneling process through a potential barrier (process 1 in Fig. 29) or a transition over point B (process 2) (Kubo and Nagamiya, 1969). At low temperatures, when the emission rate is small, process 1 is more probable than process 2. It has also been verified that enhanced emission rates are not dominated by possible thermoelastic losses of the mechanical energy.

Nonlinear effects originating from oscillating stresses in solids are of particular interest. These are (i) static strains associated with propagating acoustic waves (Cantrell, 1984; Yost and Cantrell, 1984), and (ii) changes in the equilibrium position of impurity atoms exhibiting low-frequency oscillations (Korotchenkov and Grimmeiss, 1995). Regarding static strains, the final energy state corresponding to an ionized center and a free electron is reduced in the presence of strain as shown in Fig. 29 by the dashed potential curve. The decrease in energy, ΔE_{th}, lowers the width and height of the potential barrier ABC and, hence, increases the electron emission probability. If the temperature dependence of the capture cross section is small, the change of the emission rate is obtained from the detailed balance relationship

$$e_{\mathrm{n}}^{\mathrm{t}} = \sigma_{\mathrm{n}}^{\mathrm{t}} v_{\mathrm{th}} N_{\mathrm{c}} \exp(-E_{\mathrm{th}}/kT)\,, \tag{30}$$

where $\sigma_{\mathrm{n}}^{\mathrm{t}}$ is the capture cross section, v_{th} is the thermal velocity of electrons in the conduction band, and N_{c} is the effective density of states in the conduction band. Yost and Cantrell (1984) have

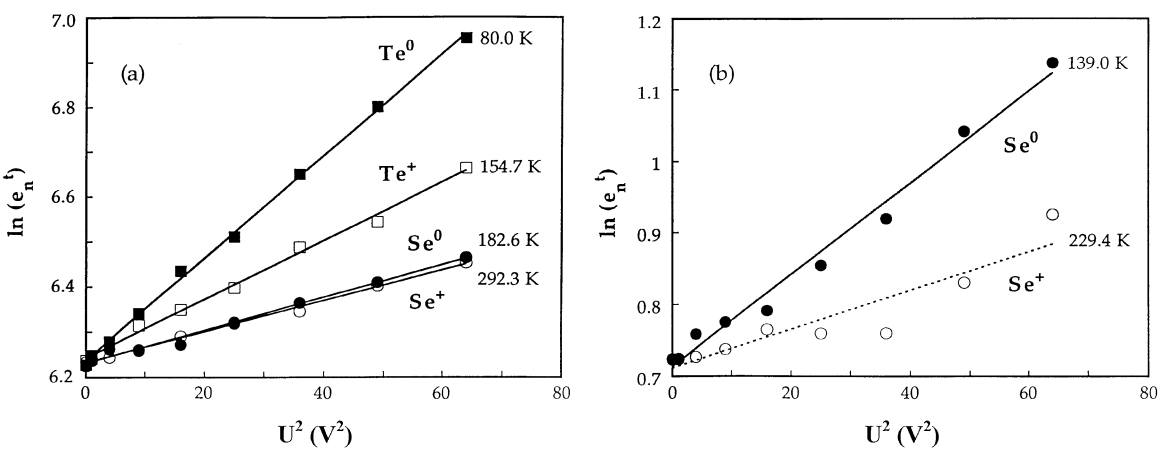

Fig. 28. Acoustically driven thermal emission rates of electrons $e_{\mathrm{n}}^{\mathrm{t}}$ at different temperatures for Se and Te centers in silicon. Lines are linear fits to the experimental data. From Korotchenkov and Grimmeiss (1995).

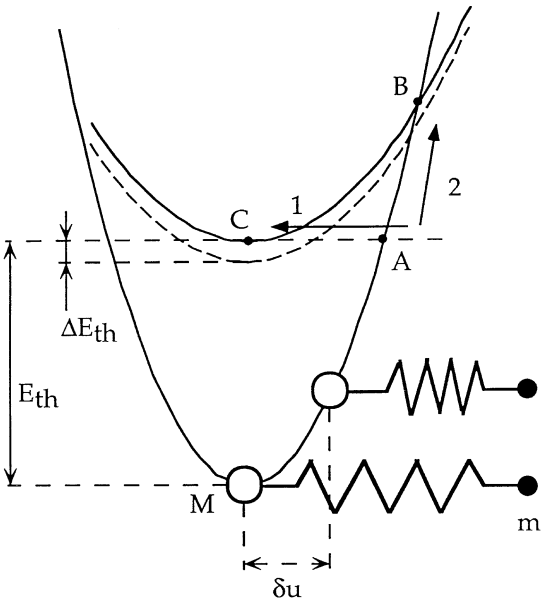

Fig. 29. Schematic energy diagram of a deep center in the adiabatic approximation. The lower curve represents the initial state with an electron captured by the impurity atom. The upper curve corresponds to an empty center and an excited electron. δu is the shift in the equilibrium position of the impurity atom M due to low-frequency vibrations at acoustic driving. m is the mass of the host atom. From Korotchenkov and Grimmeiss (1995).

argued that the strength of the static component depends on the amplitude of the applied strain squared. Considering ΔE_{th} to be a linear function of stresses and taking into account Hooke's law, one would expect a square dependence of ΔE_{th} on the amplitude of applied stresses. This implies that the change of the logarithm of the emission rate is proportional to U^2:

$$\Delta(\ln e_{\mathrm{n}}^{\mathrm{t}}) \sim \Delta E_{\mathrm{th}} \sim U^2 \ . \tag{31}$$

Fig. 28 shows that, within the scatter of the experimental data, plots of $\ln e_{\mathrm{n}}^{\mathrm{t}}$ vs. U^2 are indeed linear for different centers.

However, following the analysis of Korotchenkov and Grimmeiss (1995), it is unlikely that small values of static strains of the order of 2×10^{-12} accompanying acoustic driving can account for the observed changes of $e_{\mathrm{n}}^{\mathrm{t}}$ presented in Fig. 28. The results are better explained by relative shifts of the impurity atoms with respect to their surrounding. A nonlinear displacement δu of impurity atoms (Fig. 29) is required to give the linear dependence shown in Fig. 28. Assuming that the lattice and impurity atoms are described by a single configuration coordinate model, the change ΔE_{th} of the bottom of a potential well $V(r)$ for a bound electron is then a linear function of δu:

$$\Delta E_{\mathrm{th}} \sim V(r)\delta u \ . \tag{32}$$

Since the displacement δu arises from higher-order terms of the lattice-defect interatomic potential, one would expect ΔE_{th} to be proportional to the square of the driving amplitude U in agreement with the data shown in Fig. 28. Assuming that the observed acoustically driven variation of about

10 meV for the binding energy of the donor levels is due to a relaxation of neighboring atoms of up to 0.5%, an order of magnitude estimate gives $\delta u \sim 3 \times 10^{-3}$ nm. Such a value seems to be feasible considering the employed driving amplitudes.

Returning to our original problem, the idea of the enhanced local field strength appears to be surprisingly accurate in describing the lifetime behavior shown in Fig. 27. For example, assuming the defect displacements to be important for the generation of microfields at the exciton site, one would expect that they exhibit a square dependence of the driving amplitude (Fig. 28). This expectation is in qualitative agreement with the data presented in Fig. 27 since the increased lifetimes are only observed at rather high driving amplitudes $U \geq 55$ V. Further, a widening of the exciton trapping potential well λ can arise from sufficiently high electric fields (Blossey, 1970). Such a widening is known to broaden PL lines and cause a slight shift of the excitonic level to lower energies which is in agreement with experimental results. Therefore, the reduced exciton lifetimes shown in Fig. 27 in the region between arrows a and b probably arise from an increase of λ in Eq. (29). Obviously, both a decrease in electron–hole wave function overlap $|\psi_0|^2$ and an increase in λ takes place. Hence, an increase in the lifetime occurs when acoustic driving is applied, and thereafter a pronounced decrease in the lifetime is observed with increasing driving amplitude as seen in Fig. 27.

If anyone is tempted to challenge this model, the way to argue emerges from Raman spectroscopy measurements. Appropriate vibrational excitations are known to be very sensitive to the degree of orientational disorder of the crystal structure. In particular, impurity states can modify the group theoretical selection rules because they break the translational and point symmetry (Damen and Shah, 1971; Martin and Damen, 1971) which enhances the scattering cross section near the exciton resonance, particularly, at the I_1 bound exciton in CdS (Damen and Shah, 1971). In some cases, it has been found that minor crystal damages or a small number of crystal defects change the momentum conservation rule in such a way that an enhancement of Raman intensities or even normally Raman inactive phonons has been observed (Powell et al., 1975; Permogorov and Reznitsky, 1976). Hence, the question on the short-range interatomic disturbances at the I_1 exciton site accompanying the driving can be addressed by using resonant Raman scattering experiments.

This leads us to a discussion of the $x(yy)\bar{x}$ scattering orientation, signifying the backscattering geometry, with the incident laser beam propagating along the x-xis and the y-axis-polarization of the incident and scattered beams. In this geometry, only an E_1 LO phonon (Arguello et al., 1969) is predicted by the momentum conservation law,

$$\boldsymbol{q} = \boldsymbol{k}_\mathrm{i} - \boldsymbol{k}_\mathrm{s} , \tag{33}$$

where $\boldsymbol{q}$ is the phonon wave vector, and $\boldsymbol{k}_\mathrm{i}$ and $\boldsymbol{k}_\mathrm{s}$ are the wave vectors of the incident and scattered photons, respectively. By tuning the wavelength of the incident laser light, the enhancement of the LO Raman line near resonance of the I_1 exciton state at about 4888 Å has been observed. Despite the almost resonant character of the scattering with 4880 Å laser light presented in Fig. 30, the fundamental conservation law (cf. Eq. (33)) is preserved so that only an E_1 LO phonon is resolved in spectrum a of Fig. 30a. While no significant changes are observed for the 2LO phonon line, the LO Raman band shape changes considerably above $U = 60$ V (Fig. 30), just in the range of the lifetime decrease observed in Fig. 27. An important conclusion is that the E_1 phonon line is enhanced by a factor of 2 for the peak intensity. This increase is likely to be due to the broadening of the excitonic state λ discussed above. Indeed, these rough approximations lead to the Raman

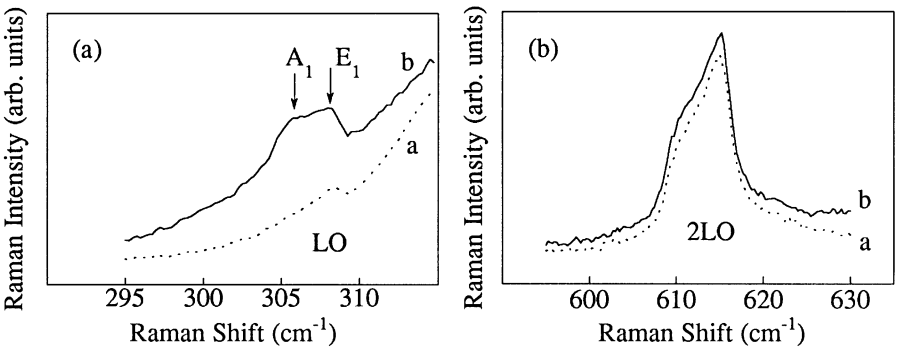

Fig. 30. Changes of the one (a) and two (b) LO Raman lines in a CdS platelet with increasing driving amplitude. Spectra a are taken without acoustic driving whereas spectra b correspond to the amplitude denoted by arrow b in Fig. 27 . The spectra a are weakly influenced at low driving amplitudes, below the value marked by arrow a in Fig. 27. Experiments are performed at 4.2 K with a 4880 Å laser light. After Korotchenkov and Goto (1998b).

cross section of the form (Leite and Porto, 1966)

$$\Xi \sim [(\omega_\alpha + \omega_0 - \omega_i)^2 + \Gamma^2]^{-1}[(\omega_\alpha - \omega_i)^2 + \Gamma^2]^{-1} , \tag{34}$$

where α refers to the I_1 bound exciton state with energy ω_α involved into the scattering process, ω_0 is the frequency of the created phonon, ω_i is the energy of the incident laser light, and Γ is the broadening parameter of the exciton state. The case with 4880 Å (2.541 eV) excitation presented in Fig. 30 is slightly off resonant with the bound exciton state at 4888 Å (2.537 eV). Therefore, the LO phonon line should increase with the broadening because of the increased coupling of the incident light ω_i to the Γ-broadened exciton state ω_α in the second determinator in Eq. (34).

A far more striking feature of the data presented in Fig. 30a is the appearance of an A_1 phonon which is polarized in the z direction (Arguello et al., 1969). This appearance is apparently contrasted with the conservation law (cf. Eq. (33)) and confirms the suggested variation of the local-crystal environment at the exciton site thus providing compelling evidence of the picture for the lifetime decrease. It is worth noting that for the two-phonon scattering the momentum conservation $\boldsymbol{q}_1 + \boldsymbol{q}_2 = \boldsymbol{k}_i - \boldsymbol{k}_s$ is now being driven by both phonons which actually does not restrict the wave vectors of the created phonons $\boldsymbol{q}_1$ and $\boldsymbol{q}_2$. Accordingly, all directions of the phonon wave vectors are likely involved in the 2LO Raman scattering process and this is fully consistent with the observation that almost no lineshape changes with increasing driving amplitude can be ascertained by analyzing the 2LO Raman lines a and b presented in Fig. 30b.

Our results on the tuning of the lifetime of bound excitons in CdS crystals should not be taken as a proof that acoustic drivings can offer a breakthrough in the lifetime engineering. The experiments we designed aimed to show a principal possibility of attaining lifetime effects with driven internal electric fields. What our results demonstrate is that the ideas of acoustic drivings seem worth extending. Can the size of the effect on the exciton lifetimes be enhanced? Do other bound exciton systems, especially quantum dot structures, show similar effects? Answering these questions will require more experiments.

7. Concluding remarks

The experimental work of the past two decades has allowed us to understand many features of the sonoluminescence effect in solids. In particular, it has become rather clear that the main consequences are the motion of dislocations imposed by intense acoustic fields and the production of vacancy-interstitials pairs of the host atoms. One of the challenges for the future will be to find atomistic-level description of the processes involved. The final model therefore is believed to eliminate the dynamical essence of point and extended defects in solids which is the topic of a long-standing challenge for the science of materials.

Our study shows that a proper understanding of acoustically driven optical effects in solids requires taking into account both the piezoelectric fields accompanying the driving and the electric fields originating from the defect charges which in turn are subject to the driving amplitude. As an attempt to extend the concept of acoustic driving, the studies on the driven exciton dynamics are outlined. As discussed in Section 6, such effects have led to the discovery of remarkably prolonged exciton lifetimes in InGaAs/GaAs quantum well structures which are due to the transportation of photogenerated carriers, electrons and holes, over macroscopic distances in the moving potential of acoustic waves. The idea of a lifetime tuning for the exciton trapped by a local potential has been demonstrated by the bound exciton complex in a CdS platelet. This suggests that microfields developed at the exciton sites become significant for understanding the results. The sources of the microfields are not universal and may be charged dislocations and/or variations of the local surroundings at the exciton site in a vibrating lattice.

Several experimental studies that have been reported in the literature provide evidence for sonoluminescence of atoms and molecules adsorbed at the crystal surface. The development of a gas discharge was tested against the electric field strengths attained with acoustic drivings. Since negative answers were obtained on the possibility of the discharge in the piezoelectric fields, the acoustically driven electric fields of dislocations become important for explaining the results.

The recently documented sonoluminescence effect in granular media leads to the possibility of truly novel insights into granular dynamics. The grain slip motions and the intergrain contact interactions revealed in sonoluminescence studies link to the fundamental properties of transportation, processing and handling of particulate solids. More work needs to be done beyond the formal description of such links.

Clearly, the developments outlined here demonstrate that the power of acoustic driving techniques for deepening our understanding of condensed matter physics cannot be overemphasized. This review stands as a call for further experiments that obviously broaden our understanding of the presented phenomena, provide new encouraging results and are thought to be of considerable practical importance.

Acknowledgements

We are indebted to many colleagues for helpful discussions on the subject of the review. The work at Kiev University was supported by the Ukrainian Ministry of Education. O.A. Korotchenkov and T. Goto wish to thank the Ministry of Education, Science and Culture of Japan for

financial support. O.A. Korotchenkov and H.G. Grimmeiss gratefully acknowledge financial support from the Swedish Institute.

References

Alzetta, G., Minnaja, N., Santucci, S., 1962. Photoluminescence in zinc-sulfide phosphors. Nuovo Cimento 23, 910–913.
Arguello, C.A., Rousseau, D.L., Porto, S.P.S., 1969. First-order Raman effect in wurtzite-type crystals. Phys. Rev. 181, 1351–1363.
Arnott, D.R., Ramsey, J.A., 1971. Electron emission from anodically oxidised aluminium due to tensile deformation. Surf. Sci. 28, 1–18.
Barber, B.P., Hiller, R.A., Löfstedt, R., Putterman, S.J., Weninger, K.R., 1997. Defining the unknowns of sonoluminescence. Phys. Rep. 281, 65–143.
Barber, B.P., Wu, C.C., Löfstedt, R., Roberts, P., Putterman, S.J., 1994. Sensitivity of sonoluminescence to experimental parameters. Phys. Rev. Lett. 72, 1380–1383.
Bastard, G., Mendez, E.E., Chang, L.L., Esaki, L., 1983. Variational calculations on a quantum well in an electric field. Phys. Rev. B 28, 3241–3245.
Benoit, J., Benalloul, P., Geoffroy, A., Balbo, N., Barthou, C., Denis, J.P., Blanzat, B., 1984. Study of highly concentrated ZnS : Mn ACTFEL devices. Phys. Stat. Sol. (a) 83, 709–717.
Blossey, D.F., 1970. Wannier exciton in an electric field. I. Optical absorption by bound and continuum states. Phys. Rev. B 2, 3976–3990.
Blossey, D.F., 1971. Wannier exciton in an electric field. II. Electroabsorption in direct-band-gap solids. Phys. Rev. B 3, 1382–1391.
Bredikhin, S.I., Shmurak, S.Z., 1979. Interaction of charged dislocations with luminescence centers in ZnS crystals. Zh. Eksp. Teor. Fiz. 76, 1028–1037 [Sov. Phys. JETP 49, 520–527 (1979)].
Burlak, G.N., Ostrovskii, I.V., 1997. Acoustic hysteresis phenomena due to the dislocation nonlinearity in crystals. Pis'ma. Zh. Tekh. Fiz. 23, 69–74 *.
Buyanova, I.A., Ostapenko, S.S., Sheinkman, M.K., Murrikov, M., 1994a. Ultrasound regeneration of EL2 centers in GaAs. Semicond. Sci. Technol. 9, 158–162.
Buyanova, I.A., Savchuk, A.U., Sheinkman, M.K., Kittler, M., 1994b. Influence of subthreshold ultrasound treatment on the recombination properties of dislocations in Ge_xSi_{1-x}-Si heterostructures. Semicond. Sci. Technol. 9, 2042–2046.
Cantrell, J.H. Jr., 1984. Acoustic–radiation stress in solids. I. Theory. Phys. Rev. B 30, 3214–3220.
Carlson, J.M., Langer, J.S., Shaw, B.E., 1994. Dynamics of earthquake faults. Rev. Mod. Phys. 66, 657–670.
Chandra, B.P., Rahangdale, Y., Ramrakhiani, M., 1990. Theory of mechanical excitation of luminescence centres in crystals. Phys. Stat. Sol. (a) 121, 281–288.
Chubachi, N., Iinuma, K., Kikuchi, Y., 1971. Influence of dislocations in CdS crystal on its electromechanical coupling factors. J. Appl. Phys. 42, 962–967.
Claytor, R.N., Brotzen, F.R., 1965. Electron emission from aluminium after low-temperature deformation. J. Appl. Phys. 36, 3549–3555.
Colbow, K., 1966. Free-to-bound and bound-to-bound transitions in CdS. Phys. Rev. 141, 742–749.
Crum, L.A., 1994. Sonoluminescence. Phys. Today 47 (9), 22–29.
Crum, L.A., Roy, R.A., 1994. Sonoluminescence. Science 226, 233–234.
Damen, T.C., Shah, J., 1971. Bound exciton resonance in Raman cross sections in CdS. Phys. Rev. Lett. 27, 1506–1508.
Dean, P.J., 1982. Photoluminescence as a diagnostic of semiconductors. Prog. Crystal Growth Charact. 5, 88–174.
Dieleman, J., Title, R.S., Smith, W.V., 1962. Paramagnetic resonance of chromium in ZnS. Phys. Lett. 1, 334–337.
Ding, J., Jeon, H., Ishihara, T., Hagerott, M., Nurmikko, A.V., Luo, H., Samarth, N., Furdyna, J., 1992. Excitonic gain and laser emission in ZnSe-based quantum wells. Phys. Rev. Lett. 69, 1707–1710.
Ermolovich, I.B., Gorbunov, V.V., Konozenko, I.D., 1977. Intrinsic defects in cadmium sulfide irradiated with thermal neutrons. Fiz. Tekh. Poluprovodn. 11, 1812–1817 [Sov. Phys. Semicond. 11, 1061–1064 (1977)].
Frenzel, H., Schultes, H., 1934. Lumineszenz in Ultraschallbeschickten Wasser. Z. Phys. Chem. Abt. B 27, 421–424.

Frommhold, L., Atchley, A.A., 1994. Is sonoluminescence due to collision-induced emission? Phys. Rev. Lett. 73, 2883–2886.
Gaitan, D.F., Crum, L.A., Roy, R.A., Church, C.C., 1992. Sonoluminescence and bubble dynamics for a single, stable, cavitation bubble. J. Acoust. Soc. Am. 91, 3166–3183.
Georgobiani, A.N., Kotlyarevskii, M.B., Mikhalenko, V.N., 1983. Intrinsic-defect luminescence centers in p-type ZnS. In: Galanin, M.D. (Ed.), Crystal Luminescence, vol. 138, Nauka, Moscow, p. 79.
Gompf, B., Günther, R., Nick, G., Pecha, R., Eisenmenger, W., 1997. Resolving sonoluminescence pulse width with time-correlated single photon counting. Phys. Rev. Lett. 79, 1405–1408.
Gorelov, B.M., Korotchenkov, O.A., Ostrovskii, I.V., Sheinkman, M.K., 1985. Ultrasonic ionization of deep centers in ZnS. Pis'ma. Zh. Tekh. Fiz. 11, 1315–1320.
Gorelov, B.M., Korotchenkov, O.A., Ostrovskii, I.V., 1989. Ultrasonic action on the paramagnetic ions in zinc sulfur crystals. Proc. 14th Conf. on Acoustoelectronics and Physical Acoustics of Solids, Kishinev, USSR, Part 1, p. 201.
Granato, A.V., Lücke, K., 1956a. Theory of mechanical damping due to dislocations. J. Appl. Phys. 27, 583–593.
Granato, A.V., Lücke, K., 1956b. Application of dislocation theory to internal friction phenomena at high frequencies. J. Appl. Phys. 27, 789–805.
Gross, E.F., Ilyinskii, A.V., Lieder, K.F., Novikov, B.V., Sokolov, N.S., 1969. Phonon-assisted exciton transitions in the spectral response of the photoconductivity of CdS single crystals. Phys. Stat. Sol. (b) 34, K59–K62.
Haff, P.K., 1983. Grain flow as a fluid-mechanical phenomenon. J. Fluid Mech. 134, 401–430.
Harada, T., Morigaki, K., 1972. Generation of free carriers via exciton–donor interaction and impact ionization of excitons in Cd(S,Se) crystals. J. Phys. Soc. Japan 32, 172–191.
Hatch, A.J., Heuckroth, L.E., 1970. Retuning effects and dynamic instability of a radio-frequency capacitive discharge. J. Appl. Phys. 41, 1701–1706.
Henry, C.H., Nassau, K., 1970. Lifetimes of bound excitons in CdS. Phys. Rev. B 1, 1628–1634 *.
Herzberg, S., 1945. Molecular Structure and Molecular Spectra, vol. I. Van Nostrand, Princeton.
Hickling, R., 1994. Transient, high-pressure solidification associated with cavitation in water. Phys. Rev. Lett. 73, 2853–2856.
Hiller, R.A., Putterman, S.J., 1995. Observation of isotope effects in sonoluminescence. Phys. Rev. Lett. 75, 3549–3551.
Hopfield, J.J., Thomas, D.G., 1961. Fine structure and magneto-optic effects in the exciton spectrum of cadmium sulfide. Phys. Rev. 122, 35–52.
Hoskins, M.J., Morkoc, H., Hunsinger, B., 1982. Charge transport by surface acoustic waves in GaAs. Appl. Phys. Lett. 41, 332–334.
Jaeger, H.M., Nagel, S.R., Behringer, R.P., 1996. Granular solids, liquids and gases. Rev. Mod. Phys. 68, 1259–1273.
Jaffrey, D., 1979. Sources of acoustic emission (AE) in metals – a review. Australasian Corrosion Eng. 23, 9–21.
James, D.R., Carpenter, S.H., 1971. Relationship between acoustic emission and dislocation kinetics in crystalline solids. J. Appl. Phys. 42, 4685–4697.
Joffe, A., 1928. The Physics of Crystals. McGraw-Hill, New York.
Joshi, S.G., White, R.M., 1969. Excitation and detection of surface elastic waves in piezoelectric crystals. J. Acoust. Soc. Am. 46, Pt. 1, 17–27.
Kalitenko, V.A., Korotchenkov, O.A., Kucherov, I.Ya., Ostrovskii, I.V., Perga, V.M., 1985. An acoustic emission induced by ultrasound in single crystals. Ukr. Fiz. Zh. (Russian edition) 30, 1358–1359.
Kalitenko, V.A., Kucherov, I.Ya., Perga, V.M., Rudenko, O.V., 1987. Acoustic emission in single crystals under dynamic loading. Fiz. Tverd. Tela 29, 2499–2501.
Kardashev, B.K., 1996. Internal friction and photoacoustic effects in II–VI and II–VII/ (HgI_2) single crystals at different levels of ultrasound strain amplitude. J. Phys. IV, Colloq. 6, 871–874.
Korotchenkov, O.A., Grimmeiss, H.G., 1995. Long-wavelength acoustic-mode-enhanced electron emission from Se and Te donors in silicon. Phys. Rev. B 52, 14598–14606 **.
Korotchenkov, O.A., Goto, T., 1997. Sonoluminescence in granular media. Phys. Rev. B 56, 13646–13649 ***.
Korotchenkov, O.A., Goto, T., 1998a. Acoustically driven bound exciton lifetimes in CdS crystals. Appl. Phys. Lett. 72 (14) in press **.
Korotchenkov, O.A., Goto, T., 1998b. Unpublished.
Koshka, J., Ostapenko, S., Ruf, T., Zhang, J.M., 1996. Activation of luminescence in polycrystalline silicon thin films by ultrasound treatment. Appl. Phys. Lett. 69, 2537–2539.

Krustok, J., 1992. Orange luminescence of donor–acceptor pairs in CdS : Ag : Cl. J. Phys. Chem. Solids 53, 1027–1030.
Kubo, R., Nagamiya, T. (Eds.), 1969. Solid State Physics. McGraw-Hill, New York.
Kulp, B.A., 1962. Displacement of the cadmium atom in single crystal CdS by electron bombardment. Phys. Rev. 125, 1865–1869.
Kulp, B.A., Kelley, R.H., 1960. Displacement of the sulfur atom in CdS by electron bombardment. J. Appl. Phys. 31, 1057–1061.
Langer, D.W., Ibuki, S., 1965. Zero-phonon lines and phonon coupling in ZnS : Mn. Phys. Rev. 138, A809–A815.
Langer, D.W., Park, Y.S., Euwema, R.N., 1966. Phonon coupling in edge emission and photoconductivity of CdSe, CdS, and $Cd(Se_xS_{1-x})$. Phys. Rev. 152, 788–796.
Leite, R.C.C., Porto, S.P.S., 1966. Enhancement of Raman cross section in CdS due to resonant absorption. Phys. Rev. Lett. 17, 10–12.
Leutwein, K., Räuber, A., Schneider, J., 1967. Optical and photoelectric properties of the F-center in ZnS. Solid State Commun. 5, 783–786.
Lord, A.E., 1975. In: Mason, W.P., Thurston, R.N. (Eds.), Physical Acoustics, vol. XI, Academic Press, New York, p. 289.
Lu, Z.H., Hanna, M.C., Szmyd, D.M., Oh, E.G., Majerfild, A., 1990. Determination of donor and acceptor densities in high-purity GaAs from photoluminescence analysis. Appl. Phys. Lett. 56, 177–179.
Lun, C.K.K., Savage, S.B., Jeffrey, D.J., Chepurniy, N., 1984. Kinetic theories for granular flow: inelastic particles in Couette flow and slightly inelastic particles in a general flow field. J. Fluid. Mech. 140, 223–256.
Lysenko, V.N., Ostrovskii, I.V., 1981a. Orange sonoluminescence of cadmium sulfide. Fiz. Tverd. Tela 23, 229–232 [Sov. Phys. Solid State 23, 129–131 (1981)].
Lysenko, V.N., Ostrovskii, I.V., 1981b. Excitation of luminescence of lithium niobate and bismuth germanate by piezoelectrically produced ultrasound. Zh. Tekh. Fiz. 51, 2155–2157 [Sov. Phys. Tech. Phys. 26, 1263–1264 (1981)].
Marinesco, M., Trillat, J.J., 1933. Action des ultrasons sur les plaques photographiques. C.R. Acad. Sci. 196, 858–860.
Martin, R.M., Damen, T.C., 1971. Breakdown of selection rules in resonance Raman scattering. Phys. Rev. Lett. 26, 86–88.
Mason, W.P. (Ed.), 1964. Physical Acoustics, vol. I-A, Academic Press, New York.
Matula, T.J., Roy, R.A., Mourad, P.D., McNamara III, W.B., Suslick, K.S., 1995. Comparison of multibubble and singlebubble sonoluminescence spectra. Phys. Rev. Lett. 75, 2602–2605.
McFee, J.H., 1966. In: Mason, W.P. (Ed.), Physical Acoustics, vol. IV-A, Academic Press, New York, p. 1.
Miyake, I., Futama, H., 1982. Sonoluminescence in X-rayed KCl crystals. J. Phys. Soc. Japan 51, 3985–3989.
Mochizuki, K., Satoh, M., Igaki, K., 1983. Orange luminescence in CdS. Japan. J. Appl. Phys. 22, 1414–1417.
Moroney, R.M., White, R.M., Howe, R.T., 1991. Microtransport induced by ultrasonic Lamb waves. Appl. Phys. Lett. 59, 774–776.
Moss, W.C., Clarke, D.B., White, J.W., Young, D.A., 1996. Sonoluminescence and the prospects for table-top micro-thermonuclear fusion. Phys. Lett. A 211, 69–74.
Mukhopadhyay, G., 1984. Effects of mechanical deformation: Exoemission. Bull. Mater. Sci. 6, 755–772.
Nasuno, S., Kudrolli, A., Gollub, J.P., 1997. Friction in granular layers: hysteresis and precursors. Phys. Rev. Lett. 79, 949–952.
Nyborg, W.L.M., 1965. In: Mason, W.P. (Ed.), Physical Acoustics, vol. II-B, Academic Press, New York, p. 265.
Onoda, G.Y., Liniger, E.G., 1990. Random loose packings of uniform spheres and the dilatancy onset. Phys. Rev. Lett. 64, 2727–2729.
Osip'yan, Yu.A., Petrenko, V.F., 1986. Physics of II–VI Compounds. Nauka, Moscow, p. 35.
Osip'yan, Yu.A., Petrenko, V.F., Zaretskii, A.V., Whitworth, R.W., 1986. Properties of II–VI semiconductors associated with moving dislocations. Adv. Phys. 35, 115–188.
Ostapenko, S.S., Bell, R.E., 1995. Ultrasound stimulated dissociation of Fe-B pairs in silicon. J. Appl. Phys. 77, 5458–5460.
Ostrovskii, I.V., 1981, Intrinsic-defect mechanism of crystal acoustoluminescence, Pis'ma. Zh. Eksp. Teor. Fiz. 34, 463–466 [JETP Lett. 34, 467–471 (1981)] ***.
Ostrovskii, I.V., Das, P., 1997. Observation of a new class of crystal sonoluminescence at piezoelectric crystal surface. Appl. Phys. Lett. 70, 167–169 ***.
Ostrovskii, I.V., Khotyaintseva, G.Yu., Vronskaya, E.V., Lysenko, V. N., 1983. Spectra of acoustoinjection luminescence in CdS crystals. Opt. Spectrosk. 54, 914–916 [Opt. Spectrosc. 54, 543–544 (1983)].

Ostrovskii, I.V., Korotchenkov, O.A., 1981. Acoustoluminescence of alkali halide crystals. Ukr. Fiz. Zh. (Russian edition) 26, 1748–1749.
Ostrovskii, I.V., Korotchenkov, O.A., 1985. Acoustooptic and acoustoelectronic detection of defects in solids. Fiz. Tverd. Tela 27, 1244–1246 [Sov. Phys. Solid State 27, 752–754 (1985)] *.
Ostrovskii, I.V., Korotchenkov, O.A., 1988. Acoustodislocation interaction under excitation of acoustoluminescence. Ukr. Fiz. Zh. (Russian edition) 33, 385–387.
Ostrovskii, I.V., Korotchenkov, O.A., 1992. Characterization of unstable point defects in crystals, Solid State Commun. 82, 267–270 **.
Ostrovskii, I.V., Lysenko, V.N., 1981. Frequency characteristics of ultrasonic luminescence of CdS resonators. Fiz. Tekh. Poluprovodn. 15, 1814–1817 [Sov. Phys. Semicond. 15, 1053–1054 (1981)].
Ostrovskii, I.V., Lysenko, V.N., 1982. Ultrasonic generation of point defects in CdS. Fiz. Tverd. Tela 24, 1206–1208 [Sov. Phys. Solid State 24, 682–683 (1982)] **.
Ostrovskii, I.V., Lysenko, V.N., 1984. Internal friction in CdS loaded by ultrasound. Fiz. Tverd. Tela 26, 531–532 [Sov. Phys. Solid State 26, 318–319 (1984)].
Ostrovskii, I.V., Lysykh, V.A., 1985. Nature of acoustoluminescence in lithium niobate. Zh. Tekh. Fiz. 55, 1460–1463 [Sov. Phys. Tech. Phys. 30, 843–845 (1985)].
Ostrovskii, I.V., Rozhko, A.Kh. 1984. Acoustic redistribution of defects in crystals. Fiz. Tverd. Tela 26, 3718–3720 [Sov. Phys. Solid State 26, 2241–2242 (1984)].
Ostrovskii, I.V., Rozhko, A.Kh., 1985. Spectra of atoms and molecules in crystal sonoluminescence. Opt. Spectrosk. 58, 395–399 [Opt. Spectrosc. 58, 236–238 (1985)] **.
Ostrovskii, I.V., Rozhko, A.Kh., Lysenko, V.N., 1979. Ultrasonic luminescence of CdS single crystals. Pis'ma. Zh. Tekh. Fiz. 5, 910 – 913 [Sov. Tech. Phys. Lett. 5, 377–379 (1979)].
Pankove, J.I., 1975. Optical Processes in Semiconductors. Dover, New York.
Permogorov, S., Reznitsky, A., 1976. Wave vector conservation in the first order resonant Raman scattering. Solid State Commun. 18, 781–784.
Petrenko, V.F., Whitworth, R.W., 1980. Charged dislocations and the plastic deformation of II–VI compounds. Philos. Mag. A 41, 681–699.
Pimbley, W.T., Francis, E.E., 1961. Effect of temperature on the exoemission of electrons from abraded aluminium surfaces. J. Appl. Phys. 32, 1729–1733.
Polland, H.-J., Schultheis, L., Kuhl, J., Göbel, E.O., Tu, C.W., 1985. Lifetime enhancement of two-dimensional excitons by the quantum-confined Stark effect. Phys. Rev. Lett. 55, 2610–2613.
Poletaev, A.V., Shmurak, S.Z., 1981. Dislocation exoemission of electrons. Pis'ma. Zh. Tekh. Fiz. 7, 1352–1355.
Poletaev, A.V., Shmurak, S.Z., 1984. Luminescence and exoemission of electrons at deformation of LiF crystals. Fiz. Tverd. Tela 26, 3567–3575 [Sov. Phys. Solid State 26, 2147–2153 (1984)].
Ponamgi, S.R., Tuan, H.-S., 1975. Excitation of surface elastic waves in a piezoelectric layered structure (by interdigital transducer). J. Acoust. Soc. Am. 57, 338–346.
Powell, D., Compaan, A., Macdonald, J.R., Forman, R.A., 1975. Raman-scattering study of ion-implantation-produced damage in Cu_2O. Phys. Rev. B 12, 20–25.
Prosperetti, A., 1997. A new mechanism for sonoluminescence. J. Acoust. Soc. Am. 101, 2003–2007.
Putterman, S.J., 1995. Sonoluminescence: sound into light. Sci. Am. 272, 32–37.
Rashba, E.I., Gurgenishvili, G.E., 1962. Edge absorption theory in semiconductors. Fiz. Tverd. Tela 4, 1029–1031 [Sov. Phys. Solid State 4, 759–760 (1962)].
Razbirin, B.S., Uraltsev, I.N., Bogdanov, A.A., 1973. Stark effect in free and bound excitons in a CdSe crystal. Fiz. Tverd. Tela 15, 878–883 [Sov. Phys. Solid State 15, 604–607 (1973)].
Redfield, D., 1963. Electric fields of defects in solids. Phys. Rev. 130, 914–915 *.
Reynolds, D.C., Litton, C.W., 1963. Edge emission and Zeeman effects in CdS. Phys. Rev. 132, 1023–1029.
Reynolds, D.C., Look, D.C., Talwar, D.N., McCoy, G.L., Evans, K.R., 1995. Demonstration of semiconductor characterization by phonon sidebands in photoluminescence. Phys. Rev. B 51, 2572–2575.
Rizakhanov, M.A., Khamidov, M.M., Abramov, I.Ya., 1978. Explanation of the features of a green-blue luminescence in ZnS by a new model of illuminating centers. Fiz. Tekh. Poluprovodn. 12, 2186–2192.
Rocke, C., Zimmermann, S., Wixforth, A., Kotthaus, J.P., Böhm, G., Weimann, G., 1997. Acoustically driven storage of light in a quantum well. Phys. Rev. Lett. 78, 4099–4102 **.

Rode, D.L., 1970. Electron mobility in II–VI semiconductors. Phys. Rev. B 2, 4036–4044.
Rosenblum, B., Bräunlich, P., Himmel, L., 1977. Spontaneous emission of charged particles and photons during tensile deformation of oxide-covered metals under ultrahigh-vacuum conditions. J. Appl. Phys. 48, 5262–5273.
Rozhko, A.Kh., 1984. Acoustoelectron emission from a piezoelectric $LiNbO_3$. Pis'ma. Zh. Tekh. Fiz. 10, 1122–1126.
Rozhko, A.Kh., Gnatenko, Yu.P., 1991. Edge luminescence of CdS : Li crystals subjected to optical and acoustic excitation. Fiz. Tverd. Tela 33, 1654–1658 [Sov. Phys. Solid State 33, 931–933 (1991)].
Samelson, H., Lempicki, A., 1962. Fluorescence of cubic ZnS : Cl crystals. Phys. Rev. 125, 901–909.
Sheinkman, M.K., Borkovskaya, L.V., Dzhymaev, B.R., Drozdova, I.A., Korsunskaya, N.E., Markevich, I.V., Singaevsky, A.F., 1995. A thermal motion of donors under ultrasound in CdS crystals. Mater. Sci. Forum 196–201, 1467–1470.
Solie, L.P., Auld, B.A., 1973. Elastic waves in free anisotropic plates. J. Acoust. Soc. Am. 54, 50–65.
Spanhel, L., Anderson, M.A., 1991. Semiconductor clusters in the sol–gel process: quantized aggregation, gelation, and crystal growth in concentrated ZnO colloids. J. Am. Chem. Soc. 113, 2826–2833.
Stearns, R.G., 1990. Ion mobility measurements in a positive corona discharge. J. Appl. Phys. 67, 2789–2799.
Swartz, J.C., Weertman, J., 1961. Modification of the Koehler–Granato–Lücke dislocation damping theory. J. Appl. Phys. 32, 1860–1865.
Taki, T., Bö, H., 1968. The decay behaviour of photoinduced ESR of Cr^+ in ZnS. J. Phys. Soc. Japan 25, 1324–1329.
Tanski, W.J., Merritt, S.W., Sacks, R.N., Cullen, D.E., 1988. Heterojunction acoustic charge transport devices on GaAs. Appl. Phys. Lett. 52, 18–20.
Thomas, D.G., Hopfield, J.J., 1959. Exciton spectrum of cadmium sulfide. Phys. Rev. 116, 573–582.
Thomas, D.G., Hopfield, J.J., 1962. Optical properties of bound exciton complexes in cadmium sulfide. Phys. Rev. 128, 2135–2148.
Tong, D.D., Goede, O., 1983. Optical study of highly Mn-doped ZnS crystals. Phys. Stat. Sol. (b) 120, K145–K149.
Truell, R., Elbaum, C., Chick, B.B., 1969. Ultrasonic Methods in Solid State Physics. Academic Press, New York.
Tyapunina, N.A., Blagoveschenskii, V.V., Zinenkova, G.M., Ivashkin, Yu.A., 1982. Features of the plastic deformation at the action of ultrasound. Izv. VUZOV, Fizika (Russian edition) 25, 118–128.
Tyapunina, N.A., Belozerova, E.P., 1988. Charged dislocations and properties of alkali halide crystals. Usp. Fiz. Nauk 156, 683–717.
Viktorov, I.A., 1967. Rayleigh and Lamb Waves. Plenum, New York.
Walton, A.J., 1977. Triboluminescence. Adv. Phys. 26, 887–948.
Walton, A.J., Reynolds, G.T., 1984. Sonoluminescence. Adv. Phys. 33, 595–660.
Wang, Y., Suna, A., McHugh, J., Hilinski, E.F., Lucas, P.A., Johnson, R.D., 1990. Optical transient bleaching of quantum-confined CdS clusters: the effects of surface-trapped electron-hole pairs. J. Chem. Phys. 92, 6927–6939.
Wen, G.W., Lin, J.Y., Jiang, H.X., Chen, Z., 1995. Quantum-confined Stark effects in semiconductor quantum dots. Phys. Rev. B 52, 5913–5922.
Whitworth, R.W., 1985. The sweep-up model of charged dislocations in ionic crystals. Philos. Mag. A 51, 857–863.
Wilson, R.B., 1966. Variation of electromechanical coupling in hexagonal CdS. J. Appl. Phys. 37, 1932–1933.
Wu, C.C., Roberts, P.H., 1993. Shock-wave propagation in a sonoluminescing gas bubble. Phys. Rev. Lett. 70, 3424–3427.
Yost, W.T., Cantrell, J.H. Jr., 1984. Acoustic-radiation stress in solids. II. Experiment. Phys. Rev. B 30, 3221–3227.
Zakrevskii, V.A., Shuldiner, A.V., 1995. Electron emission and luminescence owing to plastic deformation of ionic crystals. Phil. Mag. B 71, 127–138.
Zhmurko, A.I., Korotchenkov, O.A., Kurik, M.V., Ostrovskii, I.V., 1983. Acoustoluminescence of ZnTe crystals. Fiz. Tverd. Tela 25, 2182–2184 [Sov. Phys. Solid State 25, 1255–1256 (1983)].
Zrenner, A., Butov, L.V., Hagn, M., 1994. Long–lived excitonic ground states in GaAs/AlAs coupled quantum well structures. Semicond. Sci. Technol. 9, 1983–1988.